

# Retinal Projections in Mice With Inherited Retinal Degeneration: Implications for Circadian Photoentrainment

IGNACIO PROVENCIO,<sup>1</sup> HOWARD M. COOPER,<sup>2</sup> AND RUSSELL G. FOSTER<sup>1\*</sup>

<sup>1</sup>Department of Biology and National Science Foundation Center for Biological Timing, University of Virginia, Charlottesville, Virginia 22903

<sup>2</sup>INSERM Unité 371, Cerveau et Vision, 69500 Bron, France

## ABSTRACT

The availability of naturally occurring and transgenic retinal mutants has made the mouse an attractive experimental model to address questions regarding photoentrainment of circadian rhythms. However, very little is known about the retinal cells and the retinal projections to the nuclei of the murine circadian timing system. Furthermore, the effect of inherited retinal degeneration on these projections is not understood. In this report, we have used pseudorabies virus as a neuroanatomical tract tracer in mice to address a series of questions: Which retinal cells mediate circadian responses to light? What is the nature of the retinohypothalamic projection? What is the impact of the inherited retinal disorder, *retinal degenerate* (*rd/rd*), on the structures of the photoentrainment pathway?

Our results show that a class of retinal ganglion cell, morphologically similar to the type III ganglion cells of the rat, appears to project to central circadian structures of the mouse. They are few in number and sparsely distributed throughout the retina. The low number and broad distribution of these specialized retinal ganglion cells may be an adaptive mechanism to integrate environmental irradiance without compromising the spatial resolution required for vision. In addition, viral infection of conelike and rodlike photoreceptors and amacrinelike cells suggest that these cells may mediate or contribute to circadian responses to light.

Inherited retinal degeneration has no obvious effect on the anatomy of the retinal cells or their projections to the circadian axis. These anatomical findings are consistent with our previous findings showing that aged *rd/rd* mice are capable of regulating their circadian rhythms by light with unattenuated sensitivity. *J. Comp. Neurol.* 395:417-439, 1998.

© 1998 Wiley-Liss, Inc.

**Indexing terms:** mice; pseudorabies virus; retina; suprachiasmatic nucleus, tract tracing

In mammals, the primary circadian pacemaker resides within the suprachiasmatic nuclei (SCN) of the hypothalamus and is synchronized (entrained) to the environmental light:dark cycle by ocular photoreceptors (photoentrainment). Until recently, the mouse had not been used to any great extent to study the organization of the mammalian circadian system. However, the increased understanding of mouse genetics and the availability of mutants has made the mouse a powerful model to dissect the circadian organization of mammals. For example, mutagenized mice are being used to identify genes involved in the generation of circadian rhythms (Takahashi et al., 1994; Vitaterna et al., 1994). Mouse retinal mutants are also being studied to identify the photoreceptors of the entrainment pathway (Ebihara and Tsuji, 1980; Foster et al., 1991, 1993; Colwell and Foster, 1992; Provencio et al., 1994; Yoshimura et al., 1994; Provencio and Foster, 1995), and in this report, we

have used wild-type mice and retinal mutants to characterize the projections from the retina to central circadian and visual structures.

Grant sponsor: NIMH; Grant number: R29 MH49837; Grant sponsor: AFOSR; Grant number: 91-NL-040; Grant sponsor: NSF; Grant number: BNS-9105383; Grant sponsor: European Neuroscience Program; Grant number: 185; Grant sponsor: Human Frontier; Grant number: RG95/68; Grant sponsor: NATO; Grant number: 950334; Grant sponsor: EEC BIOMED2; Grant number: BMH4 CT 972327.

Ignacio Provencio's current address: Department of Anatomy and Cell Biology, Uniformed Services University of the Health Sciences, 4301 Jones Bridge Road, Bethesda, MD 20814.

\*Correspondence to: Dr. Russel Foster, Imperial College of Science Technology and Medicine, Department of Biology, Prince Consort Road, London SW7 2BB, UK. E-mail: r.foster@ic.ac.uk

Received 22 January 1997; Revised 8 January 1998; Accepted 20 January 1998

Mice homozygous for the *retinal degenerate* (*rd*) allele experience a degeneration of rod photoreceptors that commences within the first 2 weeks of postnatal development. This degeneration is homologous to some heritable human retinal dystrophies (McLaughlin et al., 1993, 1995). These mice also suffer a secondary, protracted degeneration of cone photoreceptors that continues into adulthood. Although rods completely degenerate by 9 weeks of age, cones lacking outer segments persist until at least 18 months (Carter-Dawson et al., 1978). The cause of cone degeneration is unknown. Rod degeneration, however, is triggered by a nonsense mutation in the gene encoding the  $\beta$ -subunit of rod-specific cGMP phosphodiesterase (Bowes et al., 1990; Farber et al., 1991; Pittler and Baehr, 1991a,b; Lem et al., 1992). This mutation elevates intracellular cGMP levels (Farber and Lolley, 1974; Farber et al., 1988) and eventually results in apoptotic cell death (Chang et al., 1993; Portera-Cailliau et al., 1994).

*Rd* mice are "visually" blind. They are incapable of learning to avoid a mild foot shock that is immediately preceded by a bright light pulse (Provencio et al., 1994). Furthermore, they show no electroretinographic (ERG) response to bright white light stimuli (Noell, 1965; Yamazaki and Suga, 1969; Provencio et al., 1994). These mutants, however, remain capable of regulating circadian rhythms by light with a sensitivity equal to or greater than that shown by congenic wild-type controls (Foster et al., 1991; Argamaso et al., 1993), and despite the progressive nature of the degeneration, the unattenuated sensitivity of the circadian system to light is maintained late in life (Provencio et al., 1994).

Photoentrainment in the *rd* mouse must be mediated through the eyes because bilateral enucleation abolishes phase shifting of circadian locomotor activity rhythms (Foster et al., 1991). However, the ocular or central mechanisms by which the sensitivity of the circadian system is maintained remains unknown. Several possibilities exist. First, very few photoreceptors may be required to maintain sensitivity, i.e., the degeneration may spare enough photoreceptors so that the photic input to the circadian system remains functionally intact. Alternatively, the photoreceptors responsible for photoentrainment may be selectively protected from the degenerative process. Finally, some compensatory mechanism within the circadian system may counteract the genetically induced damage to the retina. Such a mechanism may involve the development of new neural circuitry or changes in the efficacy of existing synapses to amplify signals weakened by the reduced sensory system (for discussion, see Foster et al., 1993).

The retinohypothalamic tract (RHT) is the pathway that conveys photic information from the retina to the two primary components of the circadian axis, the SCN and intergeniculate leaflet of the thalamus (IGL). Within the past two decades, the RHT of several species has been studied extensively. However, very little is known about the anatomical state of the RHT in animals with retinal degeneration (Colwell and Foster, 1992). Recent work in the blind mole rat (*Spalax ehrenberghi*), a subterranean rodent with small (~650  $\mu$ m in diameter) subcutaneous eyes, suggests that the RHT and its efferent structures may be unaffected by ocular regression, whereas central structures associated with visual image formation are highly degenerate (Cooper et al., 1993a,b).

Collectively, these behavioral and anatomical findings in the blind mole rat and *rd* mouse emphasize that two functionally distinct systems exist for processing light information (Pickard, 1985; Foster et al., 1991, 1993; Cooper et al., 1993b). The "image-forming" system constructs a representation of the environment by maintaining a topographical map between the retina and the central visual sites, such as the dorsal lateral geniculate nucleus (dLGN), superior colliculus (SC), and visual cortex. Components of the "non-image-forming" system, such as the SCN and IGL, are not used for image formation but rather detect changes in irradiance (Meijer et al., 1986; Harrington and Rusak, 1991; Foster, 1996).

The first objective of the present study was to characterize the retinal projections in the mouse and to assess the consequences of retinal degeneration on the anatomical state of the photoentrainment pathway. To this end, we used pseudorabies virus (PRV) as a neuroanatomical tract tracer. PRV, a porcine alphaherpes virus that causes Aujeszky's disease in livestock (Gustafson, 1975; Mettenleiter, 1991), is commonly used for viral tract tracing because its host range does not include humans. It has been shown to be highly effective in characterizing functional neural circuits (for reviews, see Strick and Card, 1992; Card and Enquist, 1995). Furthermore, several genetic variants of the field strain are available, which show different patterns of infectivity. For example, intravitreal injection of the wild-type strain Becker (PRV-Be) results in infection of image-forming and non-image-forming retinorecipient sites in the hypothalamus, thalamus, and tectum (Card et al., 1991; Enquist et al., 1994). By contrast, intravitreal injection of an attenuated strain (PRV-Ba, PRV-91, PRV-98, or PRV-99) results in selective infection of non-image-forming retinorecipient structures (Card et al., 1991; Enquist et al., 1994).

#### Abbreviations

5-HT	serotonin	OPL	outer plexiform layer
APN	anterior pretectal nucleus	OPN	olivary pretectal nucleus
contra	contralateral	OS	photoreceptor outer segments
CT-HRP	cholera toxin conjugated horseradish peroxidase	PPN	posterior pretectal nucleus
dLGN	dorsal lateral geniculate nucleus	PRT	pretectum
GC	ganglion cell layer	PRV	pseudorabies virus
IGL	intergeniculate leaflet	PRV-Ba	pseudorabies virus, Bartha strain
III	third ventricle	PRV-Be	pseudorabies virus, Becker strain
INL	inner nuclear layer	RGC	retinal ganglion cell
IPL	inner plexiform layer	RHT	retinohypothalamic tract
ipsi	ipsilateral	SC	superior colliculus
LGN	lateral geniculate nucleus	SCN	suprachiasmatic nucleus
NOT	nucleus of the optic tract	VIP	vasoactive intestinal peptide
NPY	neuropeptide Y	vLGN	ventral lateral geniculate nucleus
ONL	outer nuclear layer	VP	vasopressin

A second objective of the present study was to use PRV to identify the cellular elements in the mouse eye that may be involved in photoentrainment and to determine whether retinal degeneration affects these cells. Previous studies in several species have employed retrograde neuroanatomical tracers to identify a small subset of retinal ganglion cells (RGCs) that project to the SCN (Pickard, 1980, 1982; Murakami et al., 1989; Balkema and Drager, 1990; Moore et al., 1995). Containing such injections within the cytoarchitectural boundaries of the SCN is difficult. Fibres within the underlying chiasm may assimilate the tracer and thus label RGCs that do not project to the SCN. However, intravitreal injection of PRV-Ba results in the specific infection of the SCN and subsequent infection of RGCs in the noninjected eye (Provencio and Foster, 1993; Moore et al., 1995). This distinct subset of RGCs gives rise to the RHT (Moore et al., 1995). We have exploited this injection paradigm to identify the retinal cells that may be involved in the photoentrainment pathway of wild-type and *rd* mice and to characterise the effect of hereditary retinal dystrophy on these cells.

## MATERIALS AND METHODS

### Experimental animals

Wild-type and *rd/rd* C57BL/6J laboratory mice were bred in our animal care facility and maintained at 22°C, 50% humidity, and under a 12-hour:12-hour light:dark cycle (lights on at 0500 EST). Food and water were available ad libitum, and all treatment of animals was in strict accordance with the guidelines of the University of Virginia Animal Research Committee.

### Virus

Becker (PRV-Be) and Bartha (PRV-Ba) strains of pseudorabies virus were used in these studies. Aliquots were stored at -80°C, thawed prior to injection, and maintained at 4°C during each series of injections. Viral titers were at least  $3 \times 10^7$  plaque-forming units per milliliter. This titre has been shown to produce optimal tract tracing results in rats (Card et al., 1995). At the conclusion of an injection series, spare virus was inactivated by the addition of an equal volume of bleach.

### Virus injections

Male adult ( $284 \pm 17$  days old, mean  $\pm$  S.E.M.) wild-type ( $n = 17$ ) and *rd/rd* ( $n = 15$ ) mice were anaesthetized by intramuscular injection of ketamine hydrochloride (90 mg/kg; Ketaset, Fort Dodge Laboratories, Fort Dodge, IA) and xylazine (5 mg/kg; Rompun, Bayer Animal Health, Shawnee Mission, KS). Each animal was immediately injected with 1.0  $\mu$ l of PRV-Be ( $n = 11$ ) or PRV-Ba ( $n = 21$ ) into the vitreous body of the left eye as described by Card et al. (1991). A 26-gauge needle mounted onto a 5- $\mu$ l Hamilton syringe was used to administer the virus. After injection, animals were individually housed in clear plastic cages and maintained in conditions identical to those in the animal care facility. Any mouse exhibiting symptoms of illness or discomfort during the postinjection survival was immediately perfused as described below.

Mice were overanaesthetized with ketamine hydrochloride 66–140 hours postinjection and transcardially perfused with approximately 30 ml of warm (40°C) heparinized saline followed by at least 200 ml of Zamboni's fixative (Zamboni and de Martino, 1967; 4% paraformaldehyde

and 15% saturated picric acid in 0.01 M phosphate buffered saline [PBS], pH 7.4, 4°C) at an approximate rate of 7 ml/minute. After perfusion, brains and eyes were removed and allowed to postfix by immersion (Zamboni's fixative, 24 hours, 4°C) before immunohistochemical processing. These surgical procedures, injections, postinjection survival times, and perfusions were conducted within a Biosafety Level 2 viral facility dedicated exclusively to these studies.

### PRV immunohistochemistry

Fixed brains were sectioned in the coronal plane at 50  $\mu$ m on either a Vibratome or freezing microtome. Corneas and lenses were dissected away from fixed eyes. Some of the eyecups were cryostat sectioned at 20  $\mu$ m and thaw-mounted onto gelatin-coated slides. Before microtome and cryostat sectioning, brains and eyes were infiltrated with cryoprotectant (30% sucrose in PBS, 24 hours, 4°C). The retinas from additional eyecups were dissected free from their eyecups and immunohistochemically processed as mentioned below for wholemount analysis. All tissue was washed with PBS ( $3 \times 10$  minutes, 4°C), incubated in an ethanolic peroxide solution (50% ethanol and 3% hydrogen peroxide in PBS, 30 minutes, 4°C) to quench endogenous peroxidase activity, and then washed again with PBST (0.2% Triton X-100 [Sigma, St. Louis, MO] in PBS,  $3 \times 10$  minutes, 4°C). Tissue was subsequently incubated in blocking solution (1.5% normal goat serum [Vector Labs, Burlingame, CA] in PBST, 60 minutes, 4°C) to reduce nonspecific immunolabeling and washed with PBST ( $3 \times 10$  minutes, 4°C). Viral antigen-containing cells were detected by incubating the sections and whole retinas in a rabbit polyclonal antiserum (Rb133) raised against whole acetone-inactivated PRV (1:10,000 dilution of Rb113 in PBST containing 1.5% normal goat serum, 72 hours, 4°C). This antibody detects PRV-Be and PRV-Ba antigens. The tissue was washed (PBST,  $3 \times 10$  minutes, 20°C), incubated in a secondary antibody solution (1:100 dilution of goat anti-rabbit IgG [Vectastain Elite Kit PK-6101, Vector Labs] in PBST containing 1.5% normal goat serum, 120 minutes, 20°C), washed again (PBST,  $3 \times 10$  minutes, 4°C), incubated in a solution containing avidin DH: biotinylated horseradish peroxidase (HRP) complexes (1:100 dilution of avidin DH reagent and 1:100 dilution of biotinylated HRP reagent [Vectastain Elite Kit PK-6101, Vector Labs] in PBST, 120 minutes, 20°C), and washed with Tris buffer (0.05 M Trizma, pH 7.6,  $3 \times 10$  minutes, 4°C). The avidin DH:biotinylated HRP macromolecular complexes were localized and enhanced in the presence of the chromogen diaminobenzidine tetrahydrochloride (DAB) and divalent cations. Specifically, tissue was preincubated in a solution of DAB-nickel (0.2 mg/ml DAB and 5.0 mg/ml nickel ammonium sulfate [ $\text{NiNH}_3\text{SO}_4$ ] in Tris buffer, 10 minutes, 4°C) and transferred into an identical DAB-nickel solution containing hydrogen peroxide (0.015% hydrogen peroxide, 4°C). The reaction was visually monitored under a dissection microscope and quenched in Tris buffer (4°C). Tissue was washed again (Tris buffer,  $3 \times 10$  minutes, 4°C), and brain sections and whole retinas were mounted onto gelatin-coated slides. All slide-mounted tissue was dehydrated, cleared, and coverslipped.

### CT-HRP ocular injections

Three wild-type male mice were anaesthetized with an intramuscular injection of ketamine hydrochloride

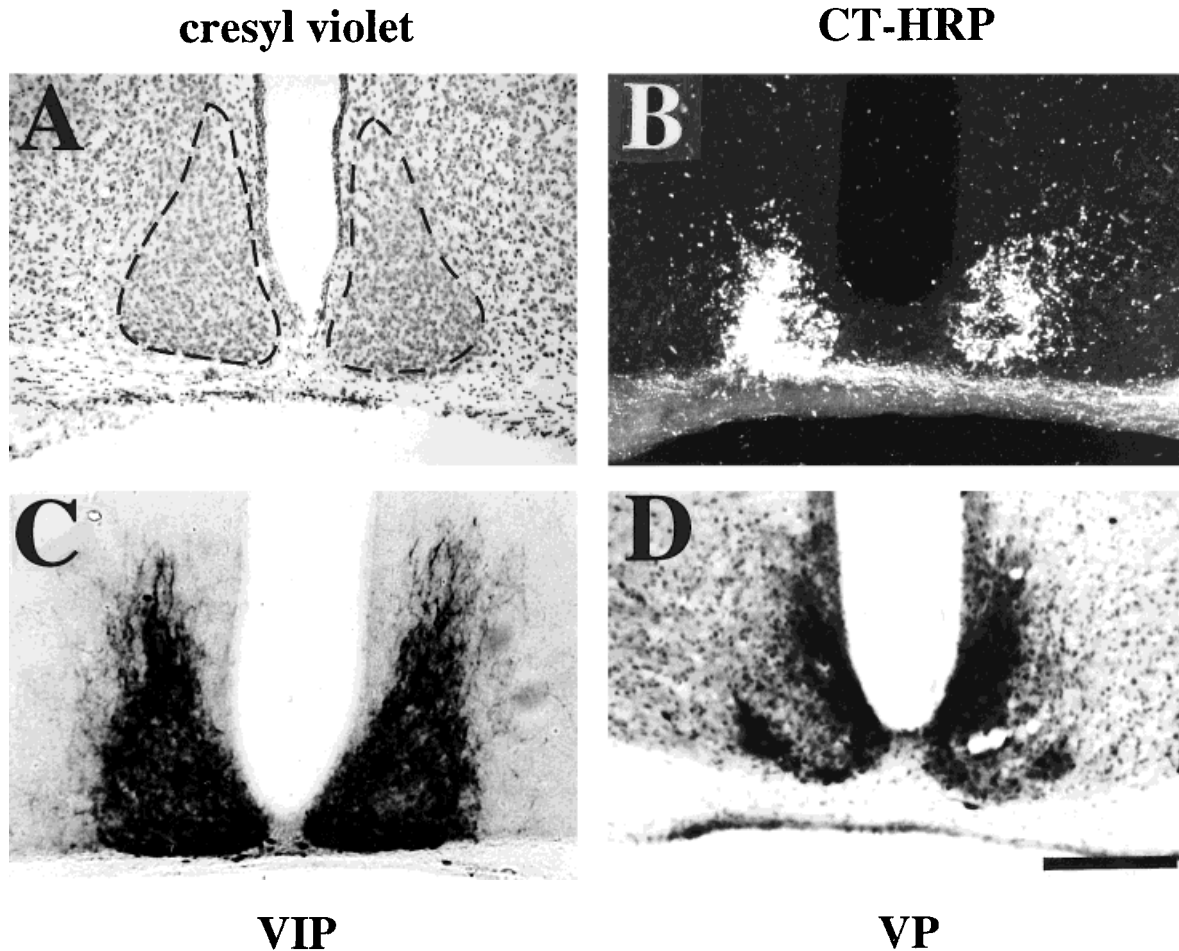


Fig. 1. Identification of the mouse suprachiasmatic nucleus (SCN). The mouse SCN was identified by using a variety of anatomical markers. **A:** The SCN are a pair of dense nuclei immediately dorsal to the optic chiasm and lateral to the third ventricle that are readily visible in cresyl violet stained coronal sections of the hypothalamus. The apparent cytoarchitectural boundaries of the nuclei are outlined by a dashed line. **B:** Retinal afferents, as demonstrated by a unilateral intravitreal injection of cholera toxin conjugated horseradish peroxidase (CT-HRP), projected bilaterally and were distributed throughout

the nucleus, with a slightly greater concentration in the ventral and lateral aspects. Ipsilateral on the darkfield photomicrograph is to the left. **C:** Vasoactive intestinal peptide (VIP)-immunopositive perikarya were predominantly located in the ventral aspect of the nuclei but were obscured by the dense plexus of VIP-positive fibers. **D:** Vasopressin (VP)-immunopositive cells were localized primarily to the dorsal periventricular and ventral aspects of the nucleus. Scale bar = 250  $\mu$ m.

(90 mg/kg; Ketaset, Fort Dodge Laboratories) and xylazine (5 mg/kg; Rompun, Bayer Animal Health). During all procedures, heart rate and respiration were monitored and body temperature was maintained at 35–36°C with a homeothermic blanket. Each animal received an intraocular injection of 3–5  $\mu$ l of 0.2% cholera toxin subunit B conjugated with HRP (CT-HRP; List Biological Laboratories, Campbell, CA). A local anesthetic (Oxybuprocaine; Chibret, Paris, France) was applied to the eye and the pupil was dilated with atropine. A small hole was made with a sharpened pipette near the ora serrata and the solution of CT-HRP was injected into the vitreous with a glass pipette (50- $\mu$ m-diameter tip) sealed to the needle of a 10- $\mu$ l Hamilton syringe. After surgery, animals received a subcutaneous injection of antibiotic (Terramycin; Pfizer, Paris, France) and were returned to their cages to recover.

The animals survived for 36 hours before perfusion. For fixation, animals received a lethal dose of sodium pentobarbital and were then perfused through the heart with

100 ml of warm saline (0.9%) followed by 400 ml of cold 4% paraformaldehyde in phosphate buffer (0.1 M, pH 7.4) and a postfixation rinse of 10% sucrose in the same buffer. Brains were removed and stored in 30% buffered sucrose at 4°C before sectioning.

For HRP histochemistry, the brains were sectioned on a freezing microtome in the coronal plane at a thickness of 40  $\mu$ m. Sections were processed with tetramethylbenzidine as a chromogen, according to the method of Mesulam (1978) as modified by Gibson et al. (1984). Sections were mounted unstained, coverslipped with depex, and observed under lightfield and darkfield illumination.

### SCN and IGL cytoarchitecture and peptide immunohistochemistry

Six mice were killed by an overdose of sodium pentobarbital and perfused with 400 ml of Zamboni's fixative (Zamboni and de Martino, 1967). The brains were dis-

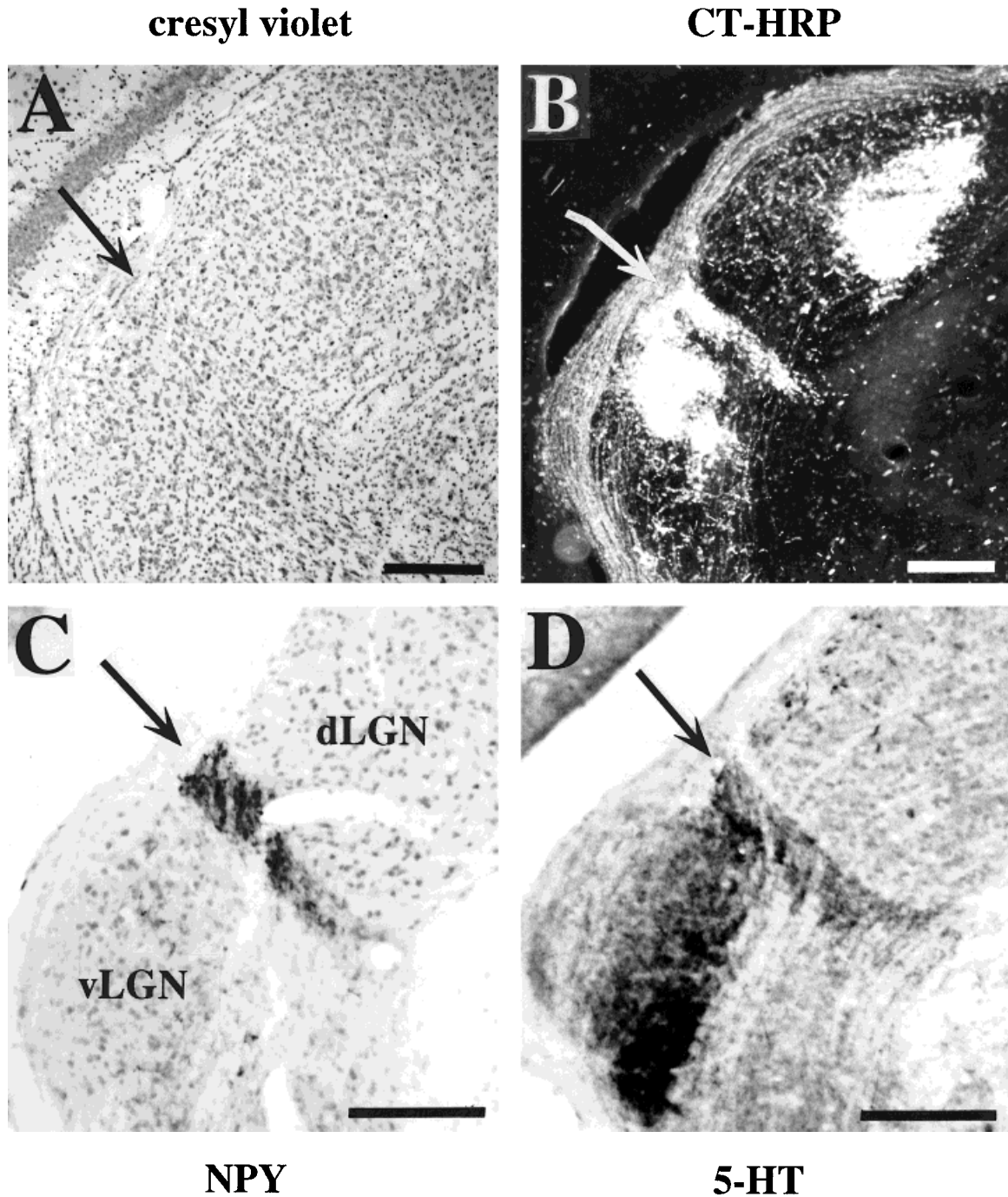


Fig. 2. Identification of the mouse intergeniculate leaflet (IGL, arrows). **A:** The IGL is very difficult to identify in cresyl violet stained coronal sections. **B:** Unilateral intravitreal injection of cholera toxin conjugated horseradish peroxidase (CT-HRP), however, resulted in dense bilateral labeling of the IGL. The darkfield photomicrograph is ipsilateral to the injected eye. Retinal afferents were observed in

sected out and postfixed overnight at 4°C in the same fixative. The brains were then immersed in 30% sucrose in phosphate buffer (0.1 M, pH 7.4) for 24 hours and subsequently frozen sectioned in the frontal plane at 30 μm.

For peptide and serotonin (5-HT) immunohistochemistry, sections were rinsed in PBS (pH 7.4, 0.1 M) containing

the dorsal (dLGN) and ventral (vLGN) lateral geniculate nuclei. **C:** Neuropeptide Y (NPY) immunoreactivity clearly delineated the IGL from the surrounding dLGN and vLGN. **D:** Serotonin (5-HT) immunoreactivity also distinguished the IGL from the ventral dLGN, but the magnocellular external division of the vLGN was also labeled. Scale bars = 150 μm.

0.3% Triton X-100 and 0.1% sodium azide (PBSTA) overnight at 4°C. Sections were transferred to phosphate buffer (0.1 M, pH 7.4) containing normal sheep serum diluted to 1:15 for 15 minutes and then placed in PBSTA with 1% hydrogen peroxide (H<sub>2</sub>O<sub>2</sub>) overnight. After a brief rinse, the sections were incubated with the primary anti-

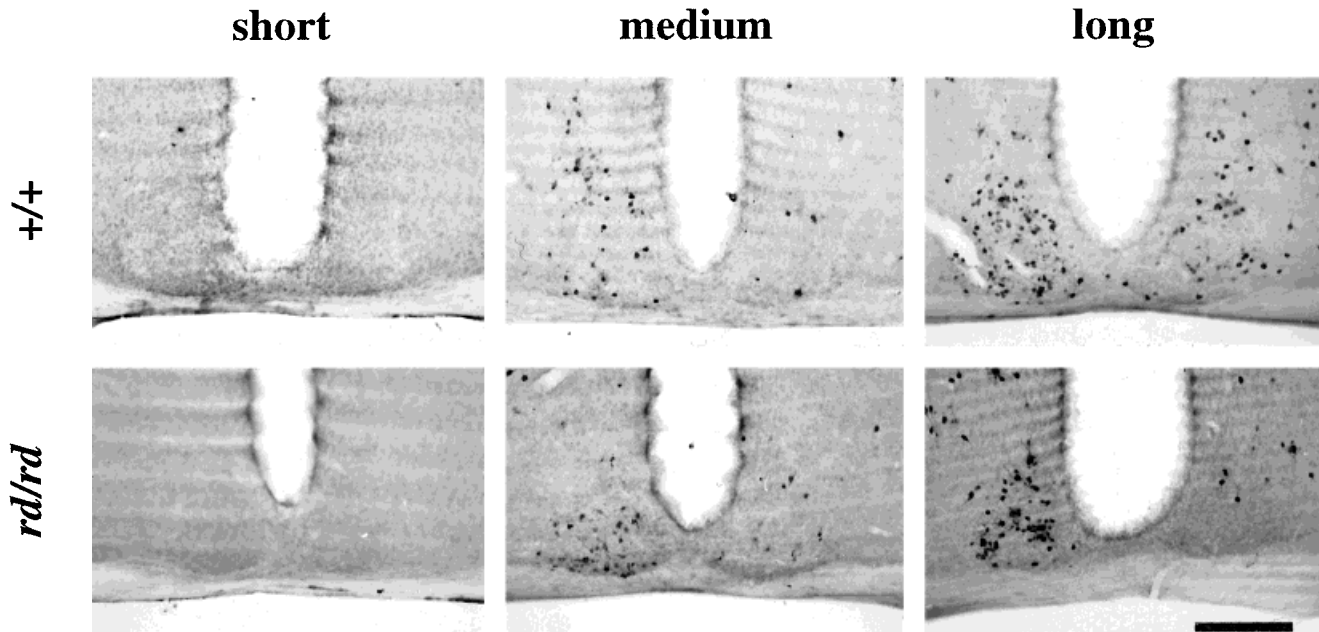


Fig. 3. Time course of infection of the suprachiasmatic nucleus (SCN) by the Bartha strain of the pseudorabies virus (PRV-Ba). The number of PRV-immunopositive cells in the SCN was directly related to postinjection survival. After a short postinjection survival time (94 hours), very few PRV-immunopositive cells could be found in the entire hypothalamus. After a medium survival time (117 hours), many more

immunopositive cells became apparent within the SCN and the surrounding anterior hypothalamus. Long survival times (<124 hours) produced maximum infection. No difference in the time course of infection was observed between wild-type and *retinal degenerate* (*rd*) mice. Ipsilateral to the injected eye is to the right. Scale bar = 250  $\mu$ m.

body and 0.1% human serum albumin in PBSTA for 5 days at 4°C. After three rinses in PBSTA, sections were transferred to sheep gamma-globulin anti-rabbit gamma globulin (INRA, Nouzilly, France) diluted to 1:300 in PBS overnight. Sections were rinsed in PBS three times and incubated overnight in peroxidase anti-peroxidase (Dako; Copenhagen, Denmark) complex diluted to 1:2,000 in PBS at 4°C. After two washes in PBS and one wash in Tris-HCl buffer (0.05 M, pH 7.9), peroxidase was reacted in the Tris buffer containing 0.02% DAB, 0.5% nickel ammonium sulfate, and 0.003% H<sub>2</sub>O<sub>2</sub> for 5–30 minutes. Sections were then briefly rinsed and mounted on gelatin-coated slides, air dried, dehydrated, cleared, and coverslipped. Alternate sections were stained for Nissl substance with cresyl violet for the purpose of cytoarchitectural observation.

The primary antibodies used were all polyclonal antisera raised in rabbit and were provided by INRA: anti-vasopressin (VP, dilution 1:3,000; Follenius and Dubois, 1979), anti-5-HT (dilution 1:15,000; Tillet et al., 1989), anti-vasoactive intestinal polypeptide (VIP, dilution 1:1,000; Moller et al., 1985), or were commercially purchased (Peninsula Labs, Paulsbo, WA; neuropeptide Y IHC 7180 [NPY], dilution 1:5,000). Specificity of staining was determined by replacing the first and second antibodies by normal rabbit serum and sheep gamma-globulin or by incubating the first antibody with saturating amounts of the homologous antigen before use.

### Neuron plotting system

Counting of labeled cells and reconstruction of cell distribution was done by using a computerized plotting system developed in the laboratory of H.M.C. The system

included a Leitz microscope equipped with a motorized XY stage. A digitized pad enabled precise displacement of the XY stage and recording of XY coordinates of the nuclear boundaries of brain structures and the location of individual cells. Data stored in files could then be used for morphometric analysis, cell counts, and serial reconstruction of sections for final illustration.

Immunolabeled cells were counted in all structures receiving retinal innervation: SCN, IGL, the dorsal and ventral geniculate nuclei (dLGN and vLGN), the pretectum (PRT), and the SC. Every section containing the SCN was counted, but this was impractical in the other structures because of the relatively larger structure volumes and number of immunopositive cells. The number of immunopositive cells from uncounted sections was estimated by interpolation. Total cell counts are the sum of actual and estimated immunopositive cell numbers for each structure.

### Ganglion cell morphology

A morphometric analysis was completed on PRV-immunopositive RGCs in the noninjected eye of wild-type and *rd* mice. Greatest diameter, equivalent diameter, surface area, and form factor were quantified from retinal wholemounts by using a charge-coupled-device camera attached to a Leitz microscope that was interfaced with a computer running image analysis software (Biocom, Les Ulis, France). Observations were made using a 50  $\times$  oil-immersion objective. Equivalent diameter ( $D_e$ ) is the diameter of a circle with an area equivalent to the surface area of the cell. It corrects for oddly shaped cells and is

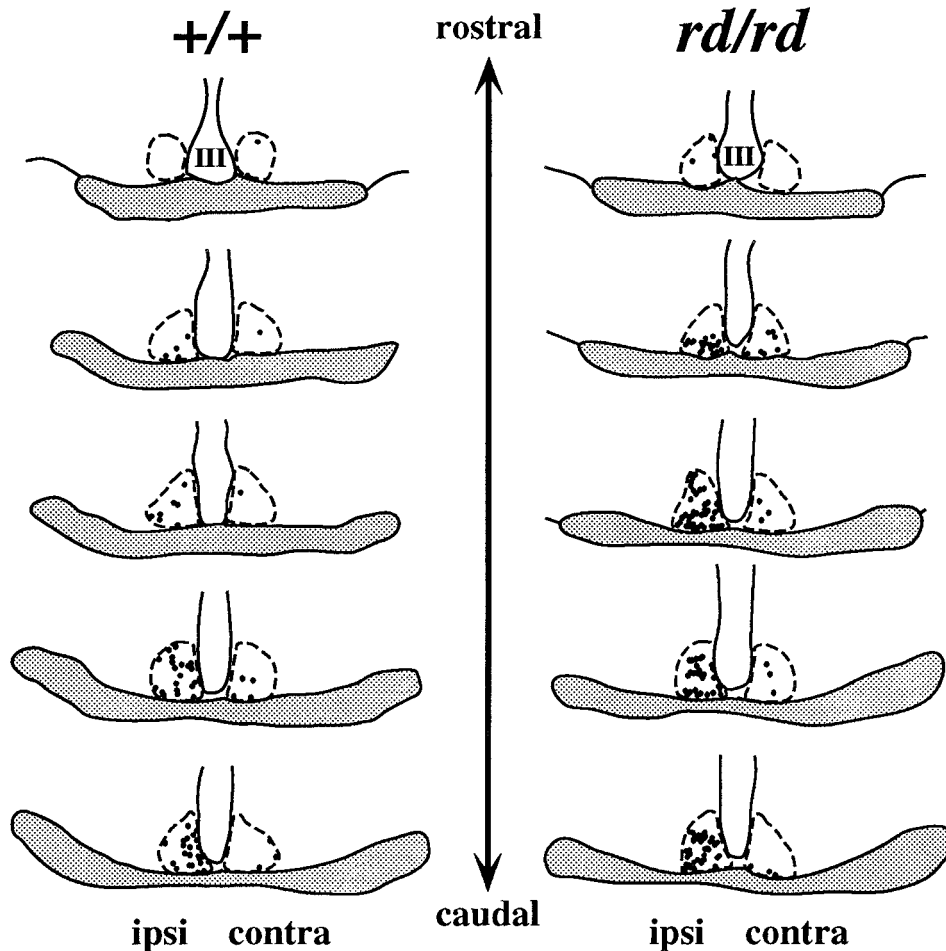


Fig. 4. Rostrocaudal distribution of the suprachiasmatic nucleus (SCN) by the Bartha strain of the pseudorabies virus (PRV-Ba). This schematic drawing is of serial coronal sections of PRV-Ba-infected hypothalami (117 hours postinjection survival) at the level of the SCN. Only those cells within the cytoarchitectural boundaries of the SCN (dashed line) were plotted. The optic chiasm is shaded, and the third

ventricle is labeled (III). Distance between consecutive sections is 50  $\mu$ m. The majority of PRV-Ba immunoreactivity was localized to the ipsilateral caudal two-thirds of the SCN. No difference in anatomical distribution was observed between wild-type and *retinal degenerate* (*rd*) mice.

calculated as follows:

$$D_e = 2 \sqrt{\frac{A}{\pi}}$$

where A = surface area of the cell. Form factor is simply the ratio of the least diameter of the cell to greatest diameter and is a useful way of describing the "ovalness" of a cell. Only those immunopositive cells clearly residing in the ganglion cell focal plane were morphometrically analyzed.

## RESULTS

### Cytoarchitecture of the SCN and IGL

To appreciate the pattern of PRV-infected neurons in the mouse hypothalamus and lateral geniculate nucleus, we first describe the retinal innervation and cytoarchitecture of these structures as demonstrated by classical anterograde tracing of CT-HRP and by the distribution of neuro-

peptide markers. The SCN is a cytoarchitecturally distinct, paired structure located in the rostral hypothalamus above the optic chiasm and below the third ventricle. In Nissl-stained sections, the SCN appears piriform in shape (Fig. 1A). The ventral expanded region of the nucleus is densely packed with small cells, whereas cell density decreases toward the dorsal pole. The distribution of retinal afferents, as demonstrated by the anterograde transport of CT-HRP, demonstrates retinal terminals distributed mainly in ventral and ventrolateral parts of the nucleus (Fig. 1B). The ventral region of the SCN contains the soma of neurons immunoreactive for VIP (Fig. 1C). The distribution of retinal terminals also partly overlaps with that of VP-immunopositive neurons located in the lateral part of the SCN. The distribution of these two populations of neuropeptide-containing cells is complementary within the SCN, with VIP-containing cells occupying the central core of the nucleus, flanked laterally and dorsally by VP-containing cells (Fig. 1D).

The IGL is one of several subdivisions of the thalamic geniculate complex. The vLGN is situated ventral to the

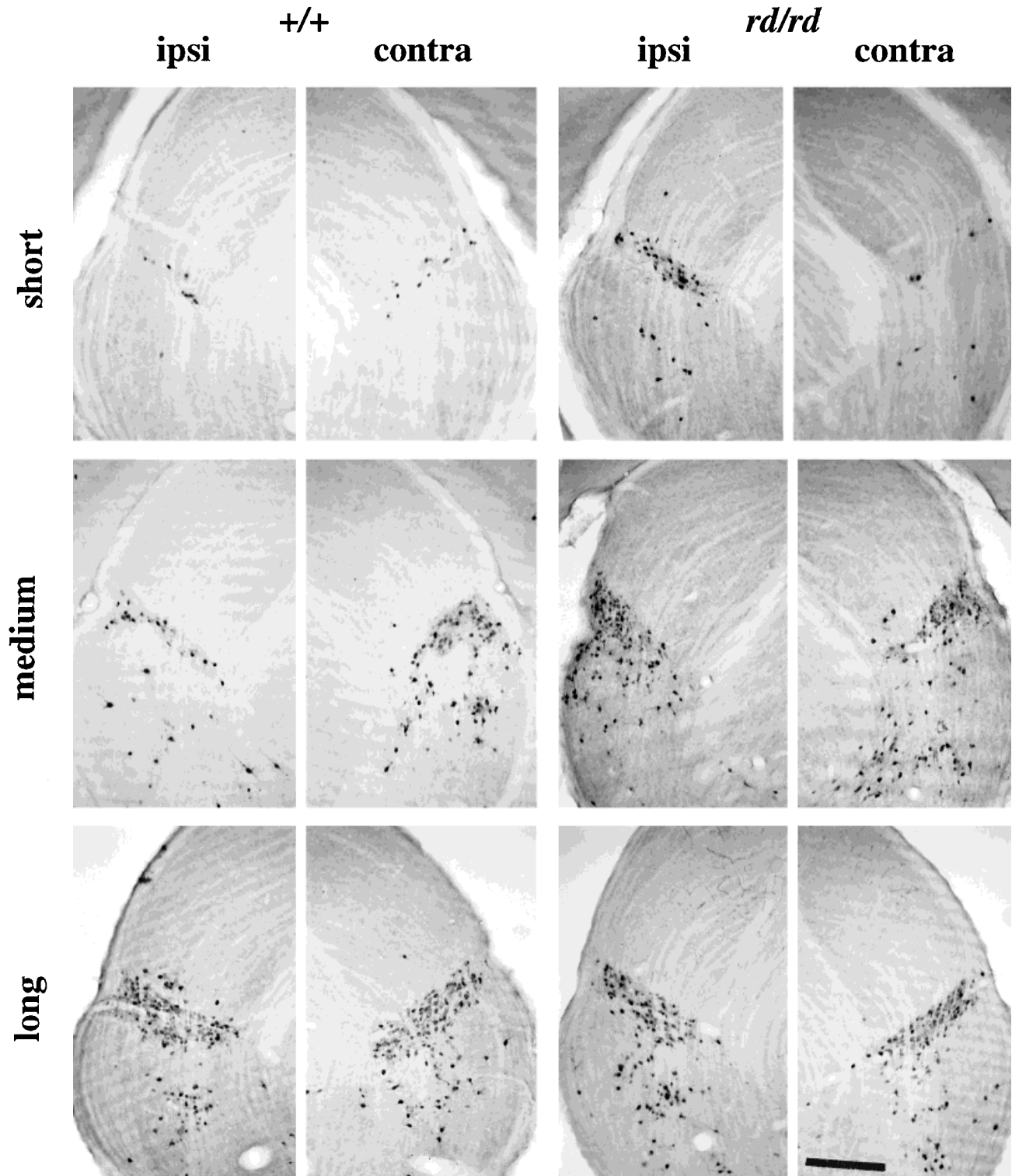


Fig. 5. Time course of infection of the intergeniculate leaflet (IGL) by the Bartha strain of the pseudorabies virus (PRV-Ba). Like the suprachiasmatic nucleus, the number of PRV-immunopositive cells in the IGL is directly related to postinjection survival. After a short postinjection survival (94 hours), relatively few PRV-immunopositive cells could be found in the geniculate. These few immunopositive cells were localized primarily to the IGL. After a medium survival time (117

hours), a greater number of cells were apparent in the IGL and ventral lateral geniculate nucleus. The longest survival times (>124 hours) produced a maximum infection. Note the absence of PRV immunoreactivity in the dorsal lateral geniculate nucleus. No difference in the time course of infection was observed between wild-type and *retinal degenerate* (*rd*) mice. Scale bar = 250  $\mu$ m.

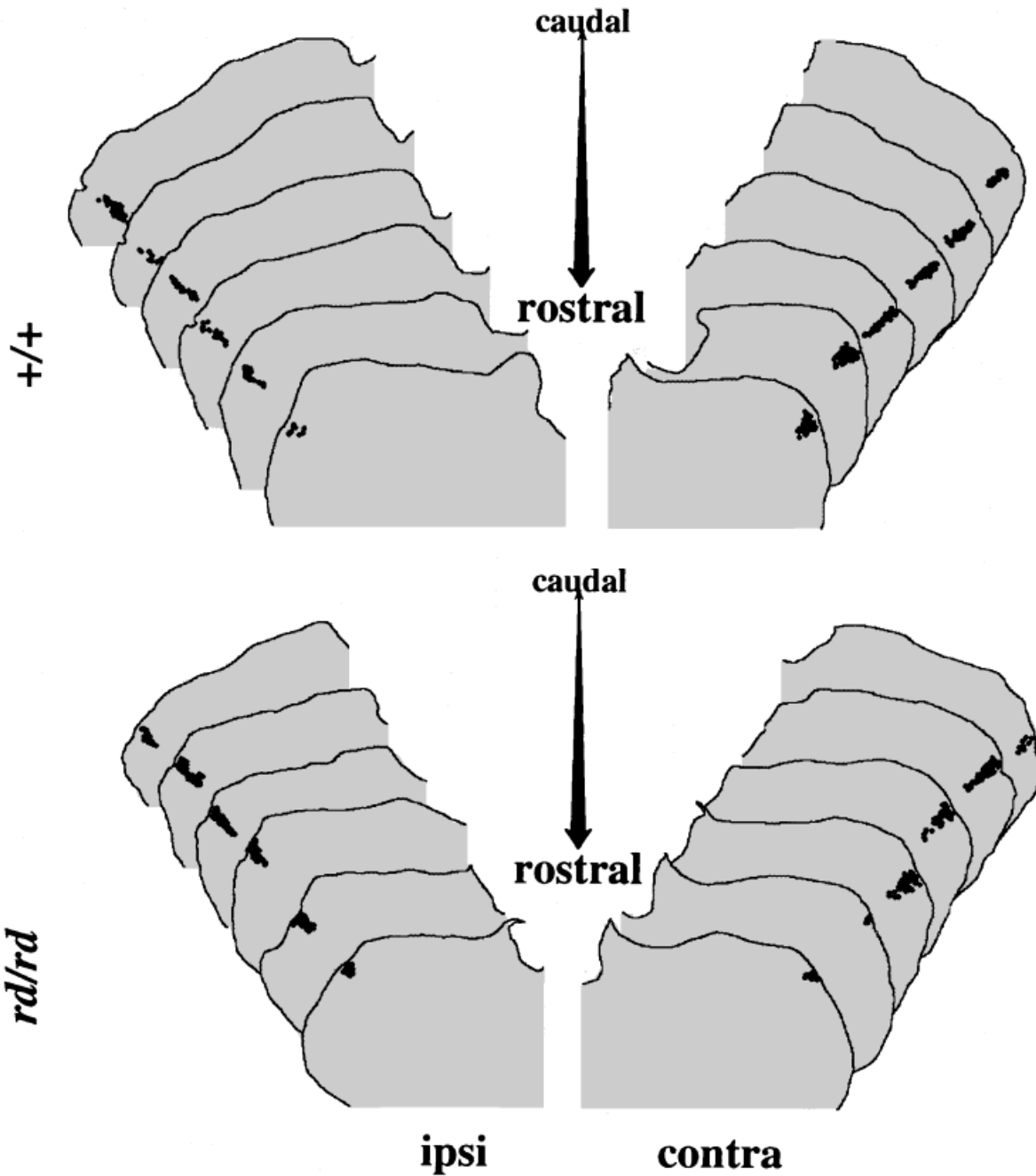


Fig. 6. Rostrocaudal distribution of the infection of the intergeniculate leaflet (IGL) by the Bartha strain of the pseudorabies virus (PRV-Ba). This schematic drawing is of serial coronal sections of PRV-Ba-infected brain (117 hours postinjection survival) at the level of the lateral geniculate. Only those cells within the IGL have been

plotted. Distance between consecutive sections is 100  $\mu$ m. The majority of PRV-Ba immunoreactivity was bilateral and throughout the rostrocaudal extent of the IGL. No differences in distribution were observed between wild-type and *retinal degenerate* (*rd*) mice.

dLGN and first appears at the level of the midregion of the dLGN (Fig. 2). The IGL, first described by Hickey and Spear (1976), is intercalated between the dorsal and ventral divisions and is the least cytoarchitecturally distinct component of the geniculate complex in Nissl-stained sections (Fig. 2A). All three geniculate subnuclei receive a retinal innervation, and the IGL can be clearly distinguished from the distribution of CT-HRP-filled antero-

grade label, especially on sections ipsilateral to the injected eye (Fig. 2B). The density of retinal innervation of the IGL in the mouse is bilaterally equivalent. The IGL stands out as an elongated triangular nucleus, obliquely oriented to the optic tract and delimiting the dorsal and ventral divisions of the geniculate complex. The cytoarchitectural distinctness of the mouse IGL is also demonstrated by the distribution of NPY-immunopositive

cells and fibers and by 5-HT-immunopositive fibers (Fig. 2C,D).

### Overview of viral infection

Wild-type and *rd* mice inoculated with PRV-Be or PRV-Ba exhibited a neuroanatomical distribution of infected cells consistent with known visual projections (Parnavelas et al., 1989) and similar to the distribution described in the rat (Card et al., 1991). Briefly, injection of PRV-Be resulted in anti-PRV-immunopositive cells within the retinorecipient structures of the hypothalamus (SCN), thalamus (dLGN, vLGN, IGL), and tectum (SC). Staining was also observed in the PRT (Fig. 8). Only a subset of these structures (SCN, IGL, vLGN, PRT) were infected after PRV-Ba injection (Fig. 7). Immunoreactivity was usually punctate in appearance and was contained primarily within the perikarya. Fibers were occasionally stained, and a few cells showed Golgi-like filling. Results in wild-type and *rd* mice were similar unless otherwise noted in the following descriptions and discussions. The results from all the animals used in this study are shown in Figure 8.

### Time course of infection

The SCN, IGL, and vLGN exhibited an increase in the number of anti-PRV-immunopositive cells as a function of postinjection survival (Figs. 3, 5, 9). This increase appeared roughly linear in the SCN but more exponential in nature within the IGL and vLGN. A high level of infection was apparent in the PRT at the earliest time points and never appeared to increase from the initially observed levels. The dLGN and SC showed virtually no immunoreactivity with PRV-Ba (Figs. 5, 7, 9).

PRV-Be injected mice showed symptoms of illness and discomfort 60–80 hours after injection. Oral and nasal secretions coupled with bouts of respiratory distress suggested that PRV-Be-injected animals suffered from pulmonary edema. Animals exhibiting these symptoms were immediately perfused even though the infection throughout the central nervous system was limited. In general, the absolute number of infected cells was lower than that found in PRV-Ba injected animals. This narrow temporal window of survival in addition to the individual variability inherent to using PRV as a transneuronal marker (Card et al., 1995) made a detailed time course analysis impossible with the PRV-Be strain.

In the rat, unilateral intravitreal injection of PRV-Be resulted in two discrete waves of infection. The first wave became apparent in the dLGN, SC, and PRT, and approximately 24 hours later, the second wave was expressed as an infection of the SCN and IGL. Rats injected with PRV-Ba never manifested this first wave but did show a robust second wave in the SCN and IGL at postinjection survival times similar to those of PRV-Be injected rats (Card et al., 1991; Card and Enquist, 1995). In the mouse as opposed to the rat, the entire progression of PRV-Be infection occurred before any appreciable infection in PRV-Ba injected mice, i.e., there did not appear to be any overlap in the complete PRV-Ba and PRV-Be time courses of infection. No obvious differences in time course, distribution, number of immunoreactive cells, or staining density were observed between the PRV-Ba-injected *rd/rd* and wild-type genotypes. In PRV-Be-injected mice, however, the number of infected cells in visual structures important in "image formation" was elevated in *rd/rd* mice relative to the wild-type mice (see Discussion).

### Central targets of PRV-Ba

**SCN.** Infection in the rostral one-third of SCN was primarily concentrated in the ventral aspect of the nucleus, but the distribution in the intermediate and caudal two-thirds was homogeneous within the cytoarchitecturally defined boundaries of the SCN (Figs. 3, 4). A few immunopositive cells in the caudal one-third could be found slightly beyond the dorsal boundaries of the nucleus. This distribution agrees with the uniquely diffuse distribution of retinal afferents described in the mouse (Cassone et al., 1988). Furthermore, longer survival time produced more immunopositive cells in the SCN, but unlike the rat, the infection never appeared to fill the nucleus completely (Card et al., 1991).

**Lateral geniculate complex.** The dLGN, vLGN, and IGL receive retinal afferents. However, PRV-Ba only labeled IGL and vLGN cells (Figs. 5, 6). No immunoreactivity was observed within the dLGN, although at longer survival times, a few positive cells near the IGL/dLGN boundary were identified (Fig. 5). The IGL proper was evenly bilaterally labeled by PRV-Ba throughout its rostro-caudal extent, a distinguishing characteristic of this structure (Hickey and Spear, 1976).

Infection within the vLGN was more pronounced at longer postinjection survival times (Figs. 5, 9) and was contained primarily within the parvocellular internal division of the nucleus. This temporal profile of infection and localization within the internal division, coupled with studies in the rat suggesting that the internal division does not receive a significant retinal input (Hickey and Spear, 1976), suggest that cells in the vLGN are not infected by a direct retinal route. Because second-order and subsequent infection is retrograde with PRV (Card et al., 1990; Card and Enquist, 1995), infected structures innervated by the vLGN may be the source of infection. The SCN and PRT receive bilateral projections from the vLGN and are both significantly infected prior to the vLGN. As a result, these areas are reasonable candidates as the source(s) of vLGN infection.

**Pretectum and tectum.** The PRT consists of at least four well-described nuclei: anterior pretectal nucleus (APN), posterior pretectal nucleus (PPN), nucleus of the optic tract (NOT), and the olivary pretectal nucleus (OPN). All except the APN receive retinally derived afferents (Scalia, 1972; Perry and Cowey, 1979). We observed viral labeling primarily within the OPN, although a few immunopositive cells were identified in the NOT and PPN (Fig. 7). Immunoreactivity was never observed within the APN. Visually differentiating between the pretectal nuclei proved difficult; therefore, all PRT infection was grouped for quantitative analysis.

Fig. 7. Infection by the Bartha strain of the pseudorabies virus (PRV-Ba) in retinorecipient structures of wild-type and *retinal degenerate* (*rd*) mice. Distribution of infection in the suprachiasmatic nucleus (SCN), lateral geniculate nucleus (LGN), pretectum (PRT), and superior colliculus (SC) 118 hours after unilateral intravitreal injection of PRV-Ba. Coronal sections (50  $\mu$ m thick) in the left column are from wild-type mice and those in the right column are from *rd* mice. SCN: Ipsilateral to the injected eye is to the left. LGN: Left panel is ipsilateral to injected eye. Note absence of immunoreactivity in dLGN. PRT and SC: Only the side contralateral to the injected eye is shown. In the PRT, the borders of the olivary pretectal nucleus (OPN) and nucleus of the optic tract (NOT) have been indicated. Note the virtual absence of infection in SC. Scale bars = 250  $\mu$ m.

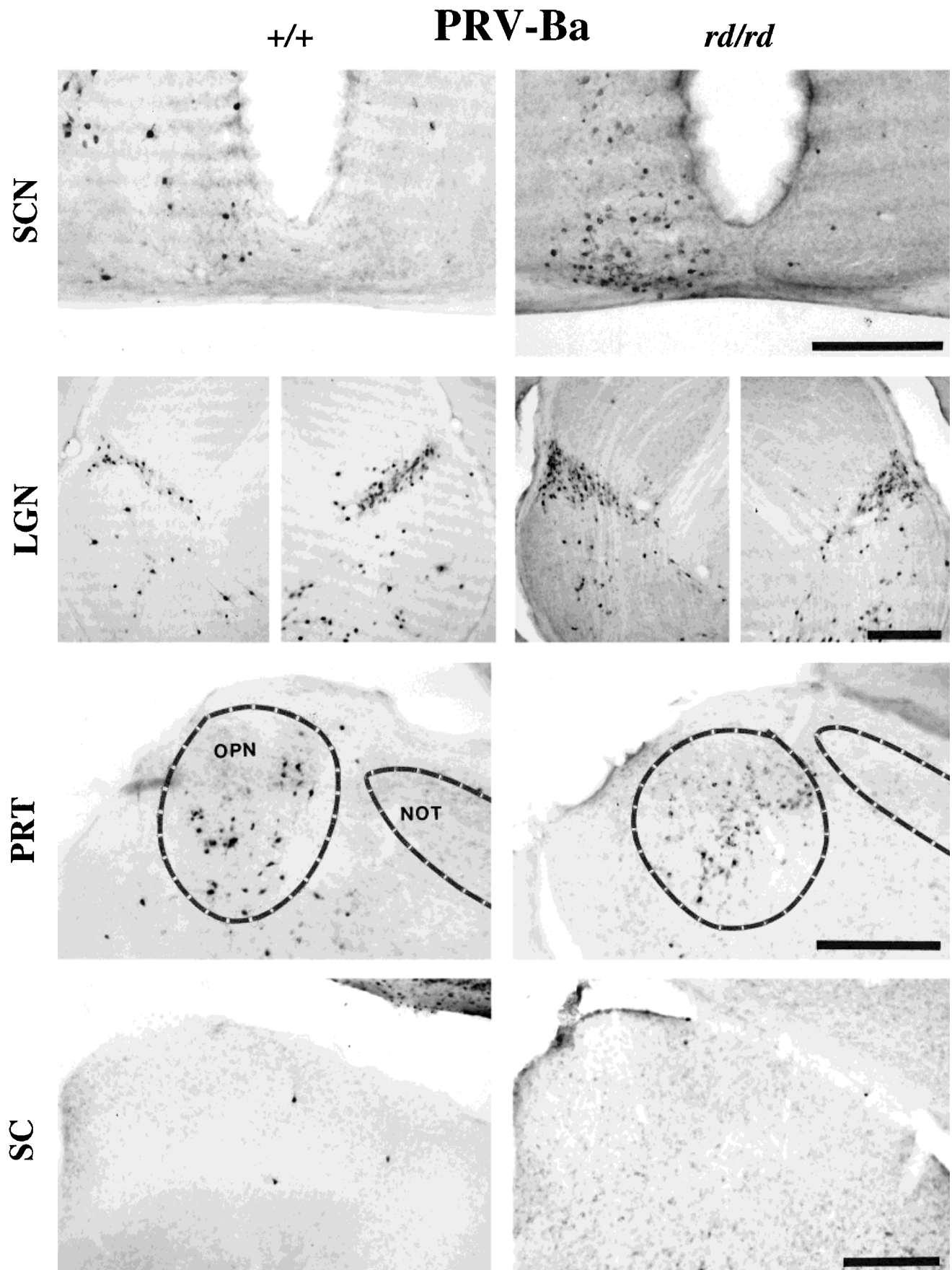


Figure 7

High levels of infection were observed at the earliest postinjection survival times (Fig. 9). This observation is similar to the rapid PRT infection observed in the rat (Card and Enquist, 1995). Infection was primarily contralateral, corresponding with the contralaterally predominant projection from the retina.

Like the dLGN, the SC, another visually mapped structure, did not show any appreciable infection from the unilateral intravitreal injection of PRV-Ba. Even survival times greater than 120 hours produced virtually no infection in the SC of *rd* or wild-type mice.

### Central targets of PRV-Ba

**SCN.** Levels of SCN infection in PRV-Ba mice rarely approached those typically observed in mice inoculated with PRV-Ba (Figs. 8, 9). These few infected cells were contained within the ventral and lateral aspects of the nucleus.

**Lateral geniculate complex.** Like the SCN, levels of IGL and vLGN infection were relatively low. The few brains containing substantial infection in these geniculate nuclei manifested a primarily contralateral distribution of infected cells. This differs from the even bilaterality observed in the IGL and vLGN of PRV-Ba-infected brains. Further, the regional distribution of infection within the vLGN was concentrated in the heavily retinorecipient magnocellular external division of the vLGN, unlike the PRV-Ba labeling of the internal division (Fig. 8).

Studies in the rat have shown that PRV-Ba selectively labels the dLGN. This "image forming" structure was also labeled in some *rd* mice, but wild-type mice never developed a substantial dLGN infection. In fact, PRV-Ba-injected wild-type mice exhibited numbers of immunoreactive dLGN cells comparable to the numbers exhibited by PRV-Ba-injected mice (Fig. 9).

**Pretectum and tectum.** A difference in infectivity between *rd* and wild-type mice was observed in the PRT and SC. This parallels the difference between wild-type and *rd* mice in the dLGN. In the PRT, immunopositive cells were localized primarily to the NOT. This distribution differs from that observed with PRV-Ba, where infection is concentrated in the OPN (Figs. 7, 8). In the SC, brains of *rd* mice exhibited dense immunoreactivity throughout the entire mediolateral extent of the superficial layer. The high density of cells made visual differentiation of individual perikarya difficult. As a result, cell counts in *rd* mice may be conservative. Wild-type brains never displayed the dense band of immunoreactivity observed in the SC of *rd* brains (Fig. 8).

### Retinal targets of PRV-Ba

PRV-Ba infection is restricted to structures involved in functions related to detection of irradiance. Immunoreactivity within the retinas of noninjected eyes must result from retrograde transport of virus from infected central structures (Moore et al., 1995). As a result, PRV-Ba can be used to label cells selectively within the retina that project to these "non-image-forming" centers. We have used this injection paradigm to label cells specifically within the retina of the noninjected eye that project to "non-image-forming" sites in the brain (Fig. 10).

**Retinal wholemount analysis.** Morphometric analysis was completed on five retinal wholemounts (two wild-type and three *rd*) from the noninjected eye of medium survival mice (112–114 hours). Fewer than 45 infected RGCs were found per retina, and these were distributed

over the entire retinal expanse (Fig. 11). Infected cell bodies had a mean greatest diameter of 11  $\mu\text{m}$ , and these cells were typically elongated in shape. Some cells were heavily labeled, which allowed visualization of the dendritic arbor proximal to the cell body. In general, cells were bipolar in nature, with two or three thin primary dendrites originating at the poles of the perikarya. These primary dendrites bifurcated within two to three cell body diameters. In general, the dendritic arbors were sparse (Fig. 12). The unimodal distribution of the four examined morphometric parameters suggests a single class of cell (Figs. 12, 13). The soma size and diffuse dendritic morphology further suggest that these RGCs are the mouse homologues of the type III ganglion cells described in the rat (Perry and Cowey, 1979; Dreher et al., 1985).

**Retinal sections.** PRV-immunoreactive cells first became apparent at medium postinjection survivals (110–120 hours). Only three classes of retinal cells became infected in wild-type and *rd* mice. The first class was localized to the ganglion cell layer and frequently displayed projections into the inner plexiform layer. Cells in this class had soma diameters of approximately 12  $\mu\text{m}$  (Fig. 14A,B). The second class of infected cells resided in the inner margin of the inner nuclear layer. This region typically contains amacrine cells. Many of these immunopositive cells had long lateral processes, and some processes could be seen penetrating into the inner plexiform layer. These cells appeared very amacrinelike in morphology (Fig. 14C–E), although we cannot preclude that these inner retinas were displaced RGCs.

The specificity of PRV-Ba and its ability to cross multiple synapses provided us with a tool to retrogradely label photoreceptors communicating with the SCN. PRV-immunopositive photoreceptors were rare, which is consistent with the low numbers of PRV-immunopositive RGCs. The retinas from the noninjected eyes of two long-survival wild-type animals contained immunoreactive outer segments of both rodlike and conelike photoreceptors. However, the immunoreactivity in the outer nuclear layer was sometimes diffuse and not contained to cell bodies, suggesting nonspecific spread of virus (Fig. 15).

## DISCUSSION

### Image-forming and non-image-forming photoreception

The mammalian eye is involved in two general types of photoreceptive tasks: image-forming and non-image-

---

Fig. 8. Infection with the Becker strain of the pseudorabies virus (PRV-Ba) in retinorecipient structures of wild-type and *retinal degenerate* (*rd*) mice. Distribution of infection in the suprachiasmatic nucleus (SCN), lateral geniculate nucleus (LGN), pretectum (PRT), and superior colliculus (SC) 78 hours after unilateral intravitreal injection of PRV-Ba. Coronal sections (50  $\mu\text{m}$  thick) in the left column are from wild-type mice and those in the right column are from *rd* mice. SCN: Ipsilateral to injected eye is to the left. Corrugated appearance of tissue is an artifact of Vibratome sectioning. LGN: Left panel is ipsilateral to injected eye. Compare presence of immunoreactivity in the dorsal LGN to the absence observed in PRV-Ba-injected mice (Figs. 5, 7). PRT and SC: Only the side contralateral to the injected eye is shown. In the PRT, the borders of the olivary pretectal nucleus (OPN) and nucleus of the optic tract (NOT) have been indicated. Note the high level of infection in external layers of SC relative to that in the PRV-Ba-injected animals (Fig. 7). Also note the greater infection in *rd* versus that in wild-type mice within "image-forming" structures (dorsal LGN and SC). Scale bars = 250  $\mu\text{m}$ .

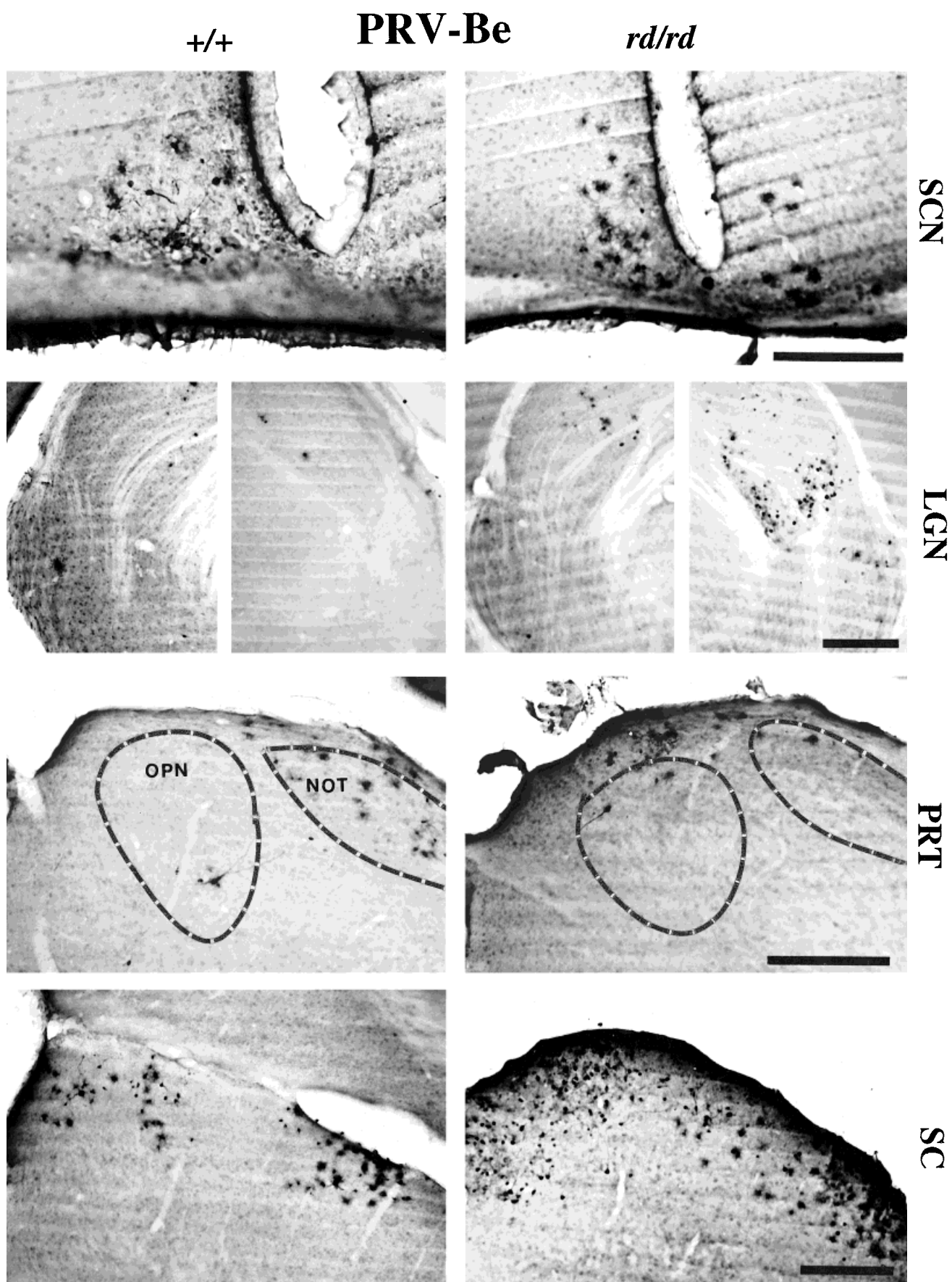


Figure 8

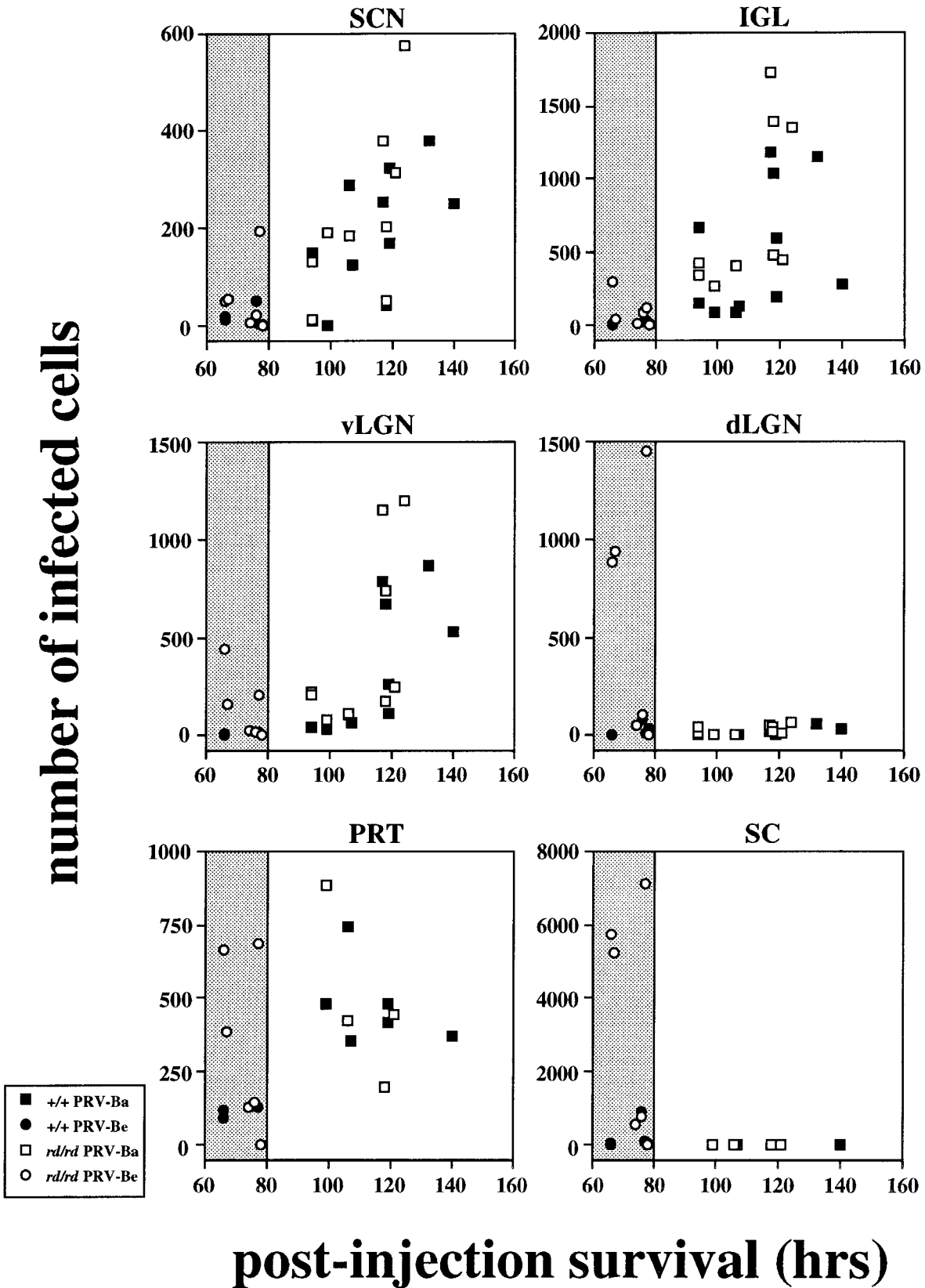


Fig. 9. Quantification of pseudorabies virus infection in retinorecipient structures as a function of postinjection survival. Data from individual animals have been plotted. Shaded portion of graphs represents the temporal window of PRV-Be infection. PRV-Ba, pseudorabies virus, Barthes strain; PRV-Be, pseudorabies virus, Becker

strain; SCN, suprachiasmatic nucleus; IGL, intergeniculate leaflet; vLGN and dLGN, ventral and dorsal lateral geniculate nuclei; PRT, pretectum; SC, superior colliculus; circles, PRV-Be-injected animals; squares, PRV-Ba-injected animals; filled symbols, wild-type mice; open symbols, *retinal degenerate (rd)* mice.

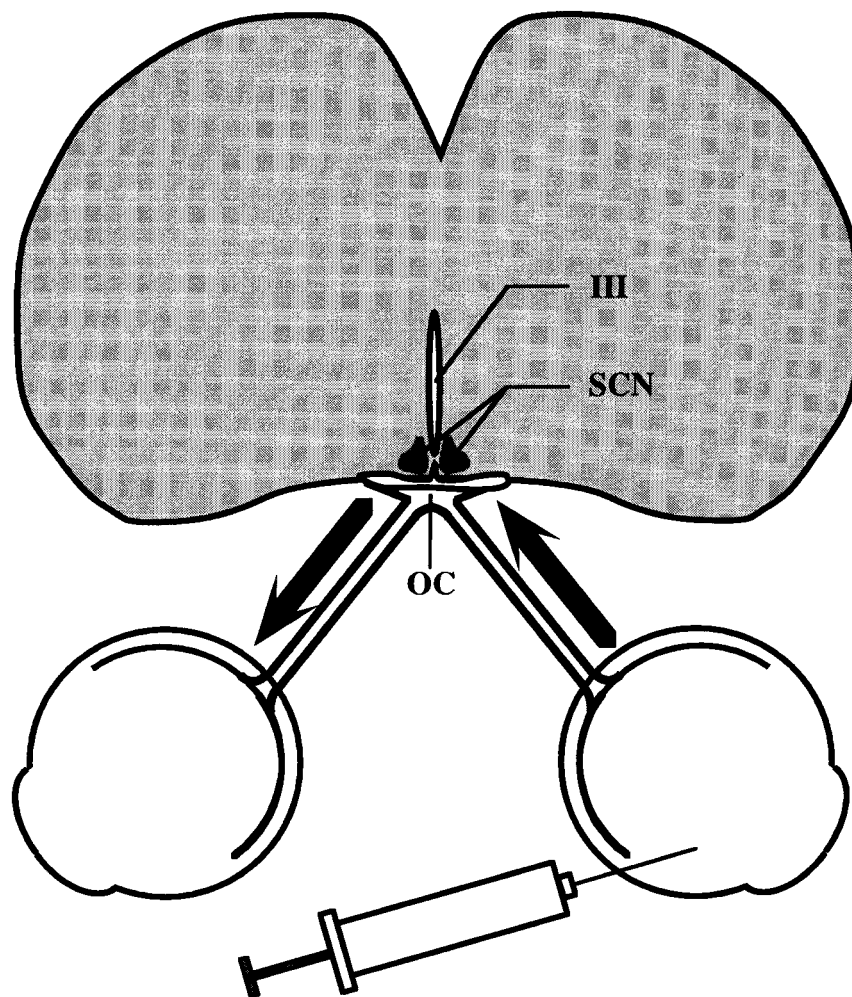


Fig. 10. Schematic of the injection paradigm used to label cells retrogradely in the noninjected eye. The Bartha strain of the pseudorabies virus was injected into the posterior chamber of one eye and subsequently transported to central "non-image-forming" retinorecipi-

ent sites in the brain (shown in coronal section) such as the suprachiasmatic nucleus (SCN; shaded). Virus was then retrogradely transported from these sites to the noninjected eye. III, third ventricle.

forming (Pickard, 1985; Foster et al., 1991, 1993; Cooper et al., 1993b). Vision, an image-forming task, requires that light be gathered to construct an accurate spatial representation of the environment. Many parameters of the visual stimulus, such as position in space, irradiance, relative motion, and color, must be collected, encoded, extracted, and processed to achieve this end. Non-image-forming tasks, such as the photic regulation of seasonal reproduction or photoentrainment of circadian rhythms, may simply require the detection of gross irradiance changes associated with dawn and dusk (Foster, 1996).

These distinct sensory tasks are anatomically segregated in the central nervous system. The image-forming visual system consists of subcortical pathways to the geniculate complex and SC. These projections are highly ordered and retinotopically mapped (for review, see Parnavelas et al., 1989). The primary nuclei of the circadian timing system are the SCN and IGL. Retinal axons reach these structures via the RHT as a retinotopically unmapped projection. Both structures contain cells that exhibit light-dependent activity, suggesting that they may

be functioning as "irradiance detectors" (Meijer et al., 1986, 1992; Harrington and Rusak, 1991). The OPN is involved in pupilloconstriction (Trejo and Cicerone, 1984; Clarke and Ikeda, 1985) and the consensual pupillary light reflex (Young and Lund, 1994). It is the only other pure "irradiance detector" identified within the mammalian nervous system (Trejo and Cicerone, 1984; Clarke and Ikeda, 1985).

The division of labor by the image-forming and non-image-forming projections is paralleled by the selective infection pattern of PRV-Ba. In the rat (Card et al., 1991) and mouse (present study), unilateral intravitreal injection of PRV-Ba results in specific labeling of the SCN, IGL, and OPN, but structures associated with image-formation, such as the dLGN and SC, do not become significantly infected. By contrast, PRV-Be infects image-forming and non-image-forming sites. PRV-Ba is also less virulent than PRV-Be, resulting in longer survival times before the appearance of discomfort or symptoms of illness. The selective infectivity and attenuated virulence of PRV-Ba

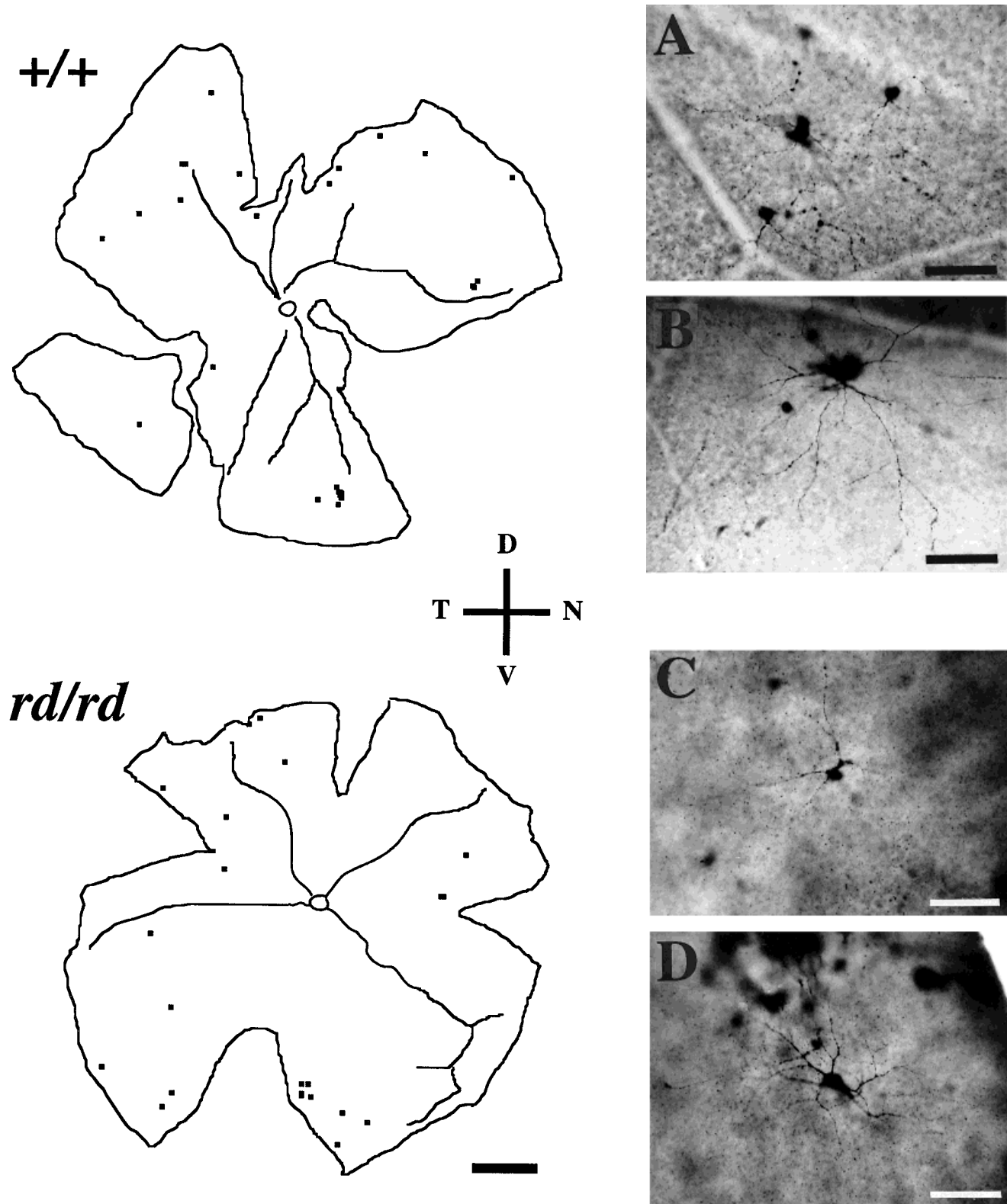


Fig. 11. Wholemount analysis of the pseudorabies virus (PRV-Ba)-infected retina in the noninjected eye. Tracings of retinas from the noninjected eyes of PRV-Ba-injected wild-type (**top**) and *retinal degenerate* (*rd*; **bottom**) mice. Small black squares indicate locations of PRV-immunopositive ganglion cells. **A**: Photomicrograph of immunore-

active ganglion cells in a wild-type retina. **B**: Immunopositive amacrine-like cell in a wild-type retina. **C**: Photomicrograph of immunoreactive ganglion cells in an *rd* retina. **D**: Immunopositive amacrine-like cell in an *rd* retina. D, dorsal; V, ventral; T, temporal; N, nasal. Scale bars = 500  $\mu$ m in wholemount tracings, 50  $\mu$ m in A–D.

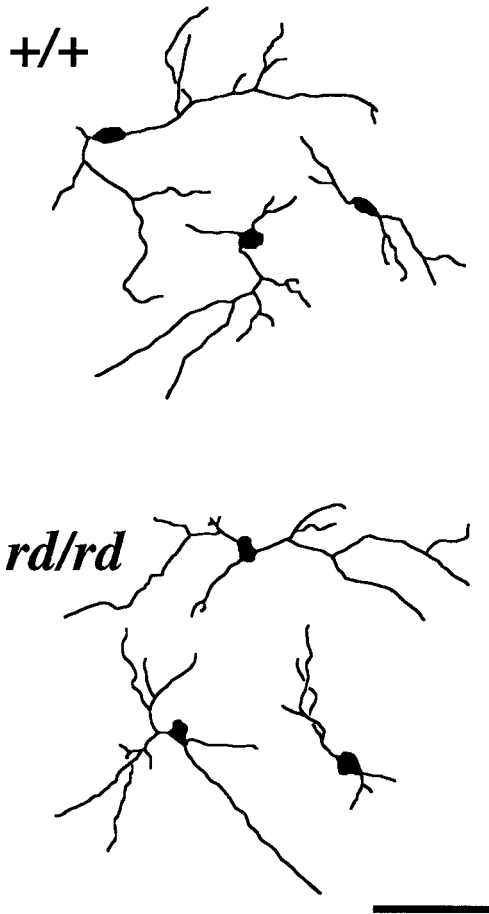


Fig. 12. Camera lucida tracings of pseudorabies virus (PRV-Ba)-positive retinal ganglion cells (RGCs) from the noninjected eye of wild-type and *rd* mice were traced. The level of dendritic labeling differed between cells. These cells are similar in morphology to the type III RGCs described in the rat. No differences were observed between the wild-type and *retinal degenerate* (*rd*) retinas. Scale bar = 50  $\mu$ m.

makes it a useful tool for tract tracing the retinal projections to non-image-forming structures.

### Comparison of PRV tract tracing in rat and mouse

This is the first PRV tract tracing study undertaken in mice. The pattern of PRV infection is similar to that found in rats (Card et al., 1991). Like the rat, PRV-Be infects all retinorecipient structures, and PRV-Ba only infects a subset of these structures that are not involved in image formation. However, despite this important similarity, a few prominent differences exist. First, the maximum postinjection survival for rats injected with PRV-Be is approximately 80 hours (Card et al., 1991). PRV-Be-injected mice also show symptoms of illness and discomfort before 80 hours, but the level PRV immunoreactivity in the central nervous system is dramatically less than that reported in the rat. Second, the postinjection survival time in PRV-Ba-injected animals is protracted relative to that observed in the rat. PRV-Ba infection could not be detected in the mouse before 94 hours after injection, and several mice

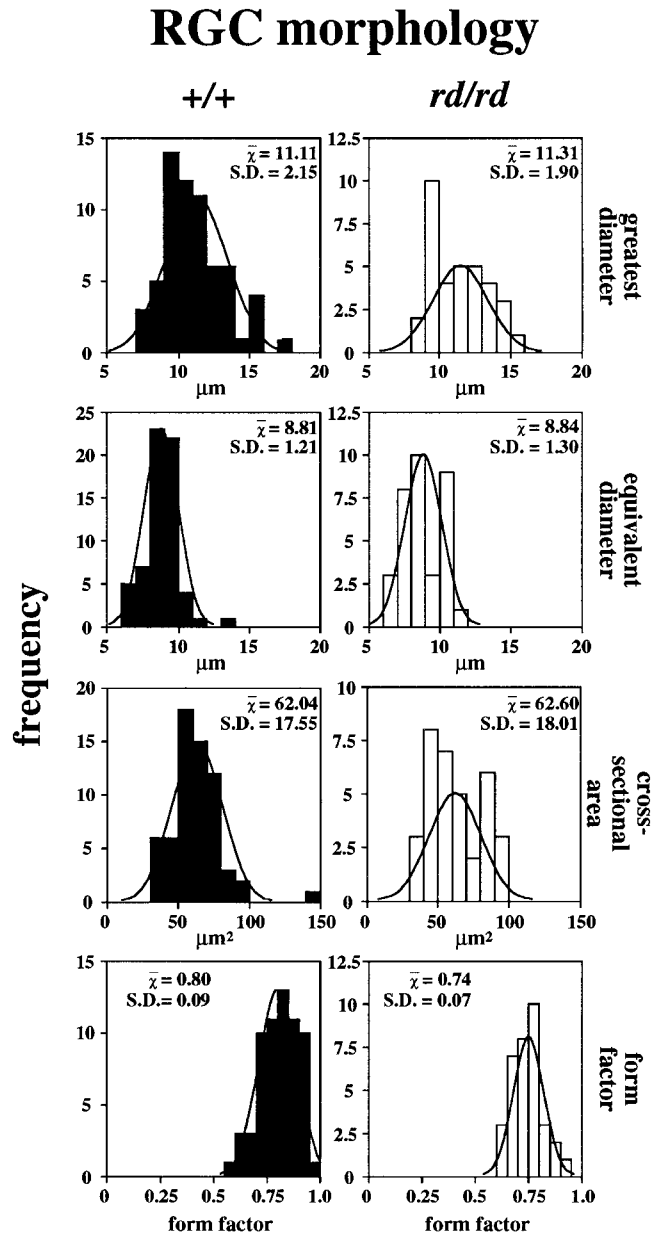


Fig. 13. Morphometric analysis of retinal ganglion cells (RGCs) positive for the pseudorabies virus, Barthes strain. Four morphometric parameters (greatest diameter, equivalent diameter, cross-sectional area, and form factor) were quantified for immunopositive RGCs in the retinas of the noninjected eyes. The normal curve defined by the mean ( $\bar{x}$ ) and standard deviation (S.D.) of each histogram has been superimposed. No difference in RGC morphology was observed between wild-type and *retinal degenerate* (*rd*) mice.

survived more the 120 hours before being perfused. Rats, however, exhibited PRV-Ba infection within the SCN and IGL 70 hours after injection and never survived more than 120 hours (Card et al., 1991). The level of infection within central structures appeared much more dense in the rat than in the mouse. At periods exceeding 100 hours, virtually every SCN neuron in the rat exhibited viral immunoreactivity (Card et al., 1991). This saturated level of infection was never observed in mice.

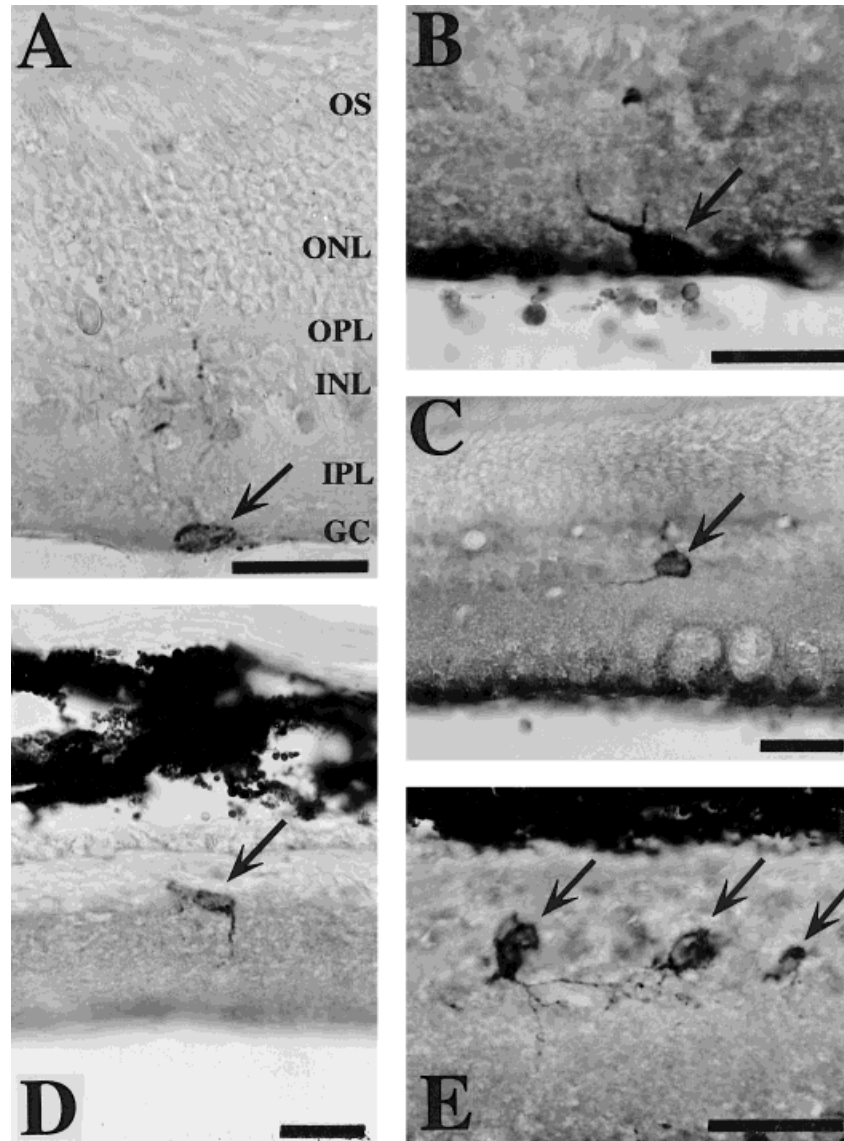


Fig. 14. Cross-sections of a retina infected with the Bartha strain of the pseudorabies virus in the noninjected eye. **A:** Immunopositive cell in the ganglion cell layer in a wild-type retina. **B:** Immunopositive cell in the ganglion cell layer in a *retinal degenerate* (*rd*) retina. **C:** Immunopositive cell in the amacrine cell sublayer of the INL in a wild-type retina. **D:** Cell similar to that shown in C but in an *rd* retina. Note the absence of outer retinal layers due to advanced retinal

degeneration. **E:** Three examples of the cells described in C and D that possess a distinct amacrinelike morphology. OS, photoreceptor outer segments; ONL, outer nuclear layer; OPL, outer plexiform layer; INL, inner nuclear layer; IPL, inner plexiform layer; GC, ganglion cell layer. Arrows indicate cells immunopositive for the pseudorabies virus. Scale bars = 25  $\mu$ m.

### Comparison of wild-type and *rd* mice

We used PRV-Ba to characterize the non-image-forming retinal projections in the mouse and to determine the effect of inherited retinal degeneration on these projections. No differences in these projections were observed between wild-type and congenic *rd* mice. This result is consistent with the finding that retinal degeneration has no effect on the ability of *rd* mice to phase shift circadian wheel running rhythms in response to pulses of light (Foster et al., 1991; Provencio et al., 1994). In fact, the sensitivity of phase shifting in the retinal mutants is indistinguishable from wild-type controls (Foster et al., 1991). Such maintenance of function suggests that the anatomical substrate (RHT) conveying photic information from the retina to the

central pacemaker (SCN) must also be intact. Although the functional status of a neural tract cannot be assessed simply by tract tracing, gross signs of degeneration (or arborization) were not obvious. Furthermore, the passage of PRV has been shown to occur through synaptically linked neurons (Dolivo et al., 1978; Rouiller et al., 1986, 1989; Strack et al., 1989a,b; Card et al., 1990, 1991, 1992; Strack and Loewy, 1990; Strick and Card, 1992; Enquist et al., 1994; Standish et al., 1994; Card and Enquist, 1995; Moore et al., 1995). Taken together, these data suggest that the *rd* mutation has no effect on the RHT.

Maintenance of non-image-forming retinorecipient nuclei has also been observed in a mammal with naturally occurring retinal degeneration. The blind mole rat, a

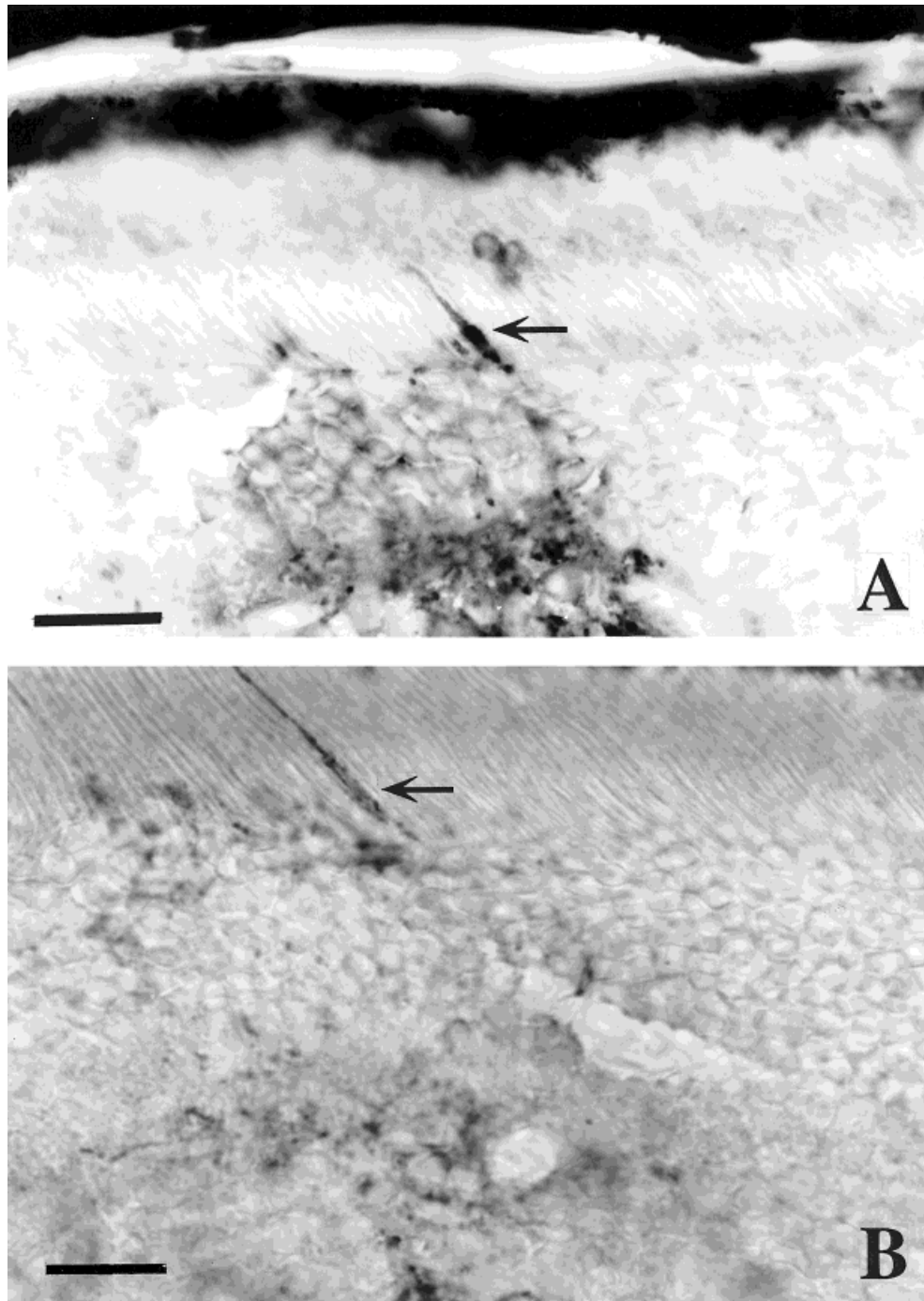


Fig. 15. Immunopositive photoreceptors in the noninjected eye. Anti-pseudorabies virus immunoreactivity was observed in the photoreceptor layer of the noninjected eye in wild-type mice. This phenomenon was only observed in two animals with very long postinjection

survival times (>136 hours). **A:** A single conelike immunopositive photoreceptor (arrow) in a cross-section (20 μm thick) of noninjected eye. Note the extensive infection in the inner retinal layers. **B:** A single rodlike immunopositive photoreceptor (arrow). Scale bars = 12 μm.

subterranean rodent with small subcutaneous eyes, has highly regressed image-forming central structures. The geniculate complex is reduced by 87–93% in volume as opposed to the volume in similar sized (120–140 g) rodents, whereas the superficial retinorecipient layers of the SC are reduced by 97%. In spite of this degenerate image-forming system, the volume of the SCN is comparable to other rodents, and the retinal projections to non-image-forming

structures are well developed (Cooper et al., 1993a,b). As a consequence of this evolutionary preservation of the circadian axis and its photic input, blind mole rats are capable of entraining locomotor rhythms to light cycles (Rado et al., 1988) and photically inducing Fos expression in the SCN (Cooper and Tobler, unpublished observations).

The number of animals injected with PRV-Be was relatively low ( $n = 13$ ). However, we observed a disparity

between wild-type and *rd* mice with respect to the number of infected retinorecipient neurons (Fig. 9). Wild-type mice exhibited relatively few infected cells in the structures that receive retinal afferents, whereas half of the *rd* mice showed substantial infection in the dLGN and SC. This may be the result of the variability inherent to this form of tract tracing (Card et al., 1995).

The observed difference in infectivity may also be a reflection of aberrant visual system development. Activity of retinal cells is important in accurate mapping of central visual structures (Goodman and Shatz, 1993; Kaprielian and Patterson, 1994; Shatz, 1994). Terminal fields of retinal afferents are focussed early in development in an activity-dependent manner to construct a precise map of visual space. The primary consequence of the *rd* mutation is the absence of rod-specific cGMP phosphodiesterase activity (Farber and Lolley, 1974, 1977; Bowes and Farber, 1987; Bowes et al., 1988, 1989, 1990; Farber et al., 1988, 1992; Pittler and Baehr, 1991a), which probably prevents rods from ever functioning. Therefore, the inactive axonal arbors in *rd/rd* mice may not be properly pruned during development. This would result in the innervation of an abnormally high number of retinorecipient neurons, which would be reflected by high levels of PRV-Be labeling in these mapped structures. PRV-Be tract tracing of dark-reared versus light-reared mice may provide insight into the observed differences within the image-forming structures of the two genotypes. Alternatively, infectivity may be inversely related to neuronal activity. RGCs that typically receive neuronal input from rod photoreceptors are probably quiescent in the *rd* mouse because of the degenerate state of the retina. Perhaps neuronal quiescence is conducive to viral replication, transport, or release. Neuronal reorganization within the retina in response to early postnatal degeneration is not well understood. Such reorganization may contribute to the differences observed in PRV-Be immunoreactivity between *rd* and wild-type mice.

### Retinal elements of the photoentrainment pathway

The specificity of PRV-Ba to non-image-forming structures has afforded us a mechanism to determine the neural elements that give rise to the RHT. After central structures became infected with PRV-Ba, viral immunoreactivity could be detected in the retina of the noninjected eye. Moore et al. (1995) showed conclusively in the rat that infected RGCs in the noninjected eye derive their infection from the SCN. These investigators accomplished this result by lesioning the optic tract just caudal to the SCN and determining the effect of this experimental manipulation on the transport of virus into the noninjected eye. They found no statistical difference in the number of infected cells in the uninjected eye between optic tract lesioned and unlesioned animals. This result strongly suggests that the infection in the uninjected eye is acquired from structures rostral to the lesioned optic tract, i.e., the SCN. It is suspected that retinal afferents from the noninjected eye incorporate, transport, and replicate the virus after it has been replicated and released from the SCN neurons (Moore et al., 1995). PRV-Ba may then retrogradely infect cells within the inner retina and potentially photoreceptors. The possibility that infected RGCs in the noninjected eye also project to other structures through collateral branches cannot be excluded. Some RGCs projecting to the SCN of the rat do have collateral branches that

TABLE 1. Retinal Ganglion Cells Afferent to the Suprachiasmatic Nucleus

Species	Number of afferent RGCs		Reference
	Ipsilateral	Contralateral	
Mouse	73 <sup>1</sup>	64 <sup>1</sup>	Balkema and Dräger (1990)
Hamster (mean ± S.D.)	46.9 ± 40.3	46.9 ± 43.0	Pickard (1982)
Cat (mean ± S.D.)	56.8 ± 19.6	258.8 ± 10.3	Murakami et al. (1989)
Sheep	<1,000	<1,000	Cooper et al. (1993)

<sup>1</sup>Data from a single animal.

continue within the optic tract (Millhouse, 1977). Although the destination of these collaterals is unknown, a population of RGCs has been identified in the hamster that projects to the SCN and IGL. These cells represent fewer than 10% of all RGCs afferent to the SCN (Pickard, 1985).

We found very few immunopositive RGCs in the noninjected eye (Fig. 11). This finding is consistent with other studies in the mouse, hamster, cat, and sheep (Table 1). Only 0.1% of axons within the rat optic nerve project to the SCN (Mason and Lincoln, 1976). The mouse retina contains 48,000–65,000 RGCs (Dräger and Olsen, 1980). Therefore, the RHT of the mouse may arise from as few as 50 RGCs. Balkema and Dräger (1990) identified approximately 70 RGCs afferent to the SCN in the mouse. Similarly, the hamster retina contains an estimated 114,000 RGCs (Tiao and Blakemore, 1976), but fewer than 150 RGCs project to the SCN (Pickard, 1982). The substantially larger cat retina (112,800–147,200 total RGCs; Stone, 1978; Stone and Campion, 1978) also contains very few (~50 ipsilaterally, ~250 contralaterally) SCN-innervating RGCs (Murakami et al., 1989). Collectively, these data indicate that the RHT is comprised of very few RGCs that are widely distributed across the retina.

Rodent RGCs have been classified into four categories based on morphology and projection (Dreher et al., 1985). Type I cells have large soma diameters (17–35 μm), a concentric dendritic arbor about 400 μm in diameter, and project to the dLGN. Type IIa RGCs have relatively small somas (10–22 μm in diameter) and small (<250 μm in diameter) “bushy” dendritic arbors. These cells project to the dLGN and SC. Type IIb cells resemble type IIa cells in their bushy appearance but differ in soma size (7–15 μm), have a smaller dendritic arbor (<140 μm), and project exclusively to the SC. Type III cells are the most morphologically heterogeneous class but can be easily recognized by the broad extent of their dendritic field. Some type III cells have dendritic arbors more than half a millimeter in diameter. The sparse morphology of the arbor, arising from few primary dendrites, is also highly characteristic of this cell type. Type III cells project primarily to the dLGN and SC.

The PRV-immunopositive cells we observed within the RGC focal plane of the noninjected eye were type III in morphology (Fig. 12). Type III cells are also the only class of RGCs shown to project to the SCN and IGL (Moore et al., 1995). Furthermore, this class of RGC is the morphological correlate of the functionally defined W-cells. At least one subtype of W-cell is tonic and fires in an irradiance-dependent manner (Rodieck and Brening, 1983). On the basis of our data, the type III ganglion cells also appear to transduce and transmit environmental irradiance levels to the SCN, IGL, and OPN of the mouse.

We also consistently found in wild-type and *rd/rd* mice immunopositive cells within the inner margin of the inner

nuclear layer that were amacrinelike in morphology (Fig. 14C–E). To our knowledge, this is the first identification of a cell in the amacrine cell layer of the retina that may be involved in the retinal input to the circadian system. There were no obvious differences in either the number or pattern of arborization in these cells between wild-type and *rd/rd* mice. Rod bipolar cells do not directly synapse on RGCs but rather transmit rod information through AII amacrine cells to cone bipolar cells, which eventually synapse on RGCs (Mills and Massey, 1995).

Virus infection in long-survival PRV-Ba-injected wild-type mice occurred in both conelike and rodlike photoreceptors (Fig. 15). Our previous results have shown that rod photoreceptors are not required for photoentrainment (Foster et al., 1991). Further, our spectral sensitivity studies have implicated both the short wave-length-sensitive cones (UV-cones,  $\lambda_{\max} = 359$ ) and middle wave-length-sensitive cones (M-cones,  $\lambda_{\max} = 511$ ) in mediating photoentrainment in *rd* mice (Provencio and Foster, 1995). However, the presence of infected rodlike photoreceptors in wild-type mice suggests that under normal circumstances rods may also contribute to circadian regulation and that there may be considerable redundancy of photoreceptor input to the circadian system. The circadian system may be capable of using any available photoreceptors to achieve photoentrainment. Alternatively, we cannot exclude the possibility that there may have been a nonspecific spread of virus within the retina, resulting in the nonspecific infection of rod photoreceptors (Fig. 15). We are currently evaluating the role of rods in photoentrainment by exploring circadian responses to light in transgenic mice that lack cone photoreceptors.

### Functional considerations

The expansive topography of the SCN-innervating RGCs may be highly adaptive. Maintenance of retinotopic organization is not necessary for irradiance detection. In fact, active scrambling of spatial information may be advantageous (Cooper et al., 1993c). A feature commonly found in irradiance measuring instruments is an integrating sphere. The role of this component is to integrate (sum) light from a broad capture field and, in effect, eliminate positional information. The eye does not contain an analogous device because it is also involved in image formation, which requires preservation of spatial information.

The type III retinal ganglion cells projecting to the SCN have the largest dendritic arbor and consequently the largest receptive field of all the ganglion cell types (Perry, 1979; Dreher et al., 1985). They are also few in number, are distributed over the entire retinal expanse, and send a retinotopically unmapped projection to the SCN (Moore and Lenn, 1972; Pickard, 1980, 1982; Murakami et al., 1989; Balkema and Drager, 1990; Moore et al., 1995). These anatomical features may provide a broad-capture and integrated input to the SCN without interfering with the eye's other function of image detection. Furthermore, this spatial integration would serve to "dilute" photons from bright point sources, such as the moon or stars, which cannot serve as reliable time cues and thus potentially interfere with stable entrainment to the solar day.

### CONCLUSIONS

This is the first study in mice to employ PRV as a neuroanatomical tracer. Our results show that PRV-Ba is a

useful tool to analyze the retinal projections to non-image-forming central structures. We have used this tracer to assess the state of the RHT in mice with inherited retinal degeneration, and we conclude that retinal degeneration has no obvious effect on the anatomical integrity of this pathway. This viral tracer was also used to identify the cells within the mouse retina that may mediate the transmission of photic information to the SCN. We found that the RHT of the mouse is comprised of very few RGCs that are widely distributed over the retina. These RGCs are type III in morphology and have broad dendritic arbors. The sparse distribution of these RGCs may provide the retina with a mechanism of integrating environmental light levels for the circadian system without sacrificing the spatial resolution required by the visual system. The infection of conelike, rodlike, and amacrinelike cells suggests that these cells may form part of the circadian entrainment pathway.

### ACKNOWLEDGMENTS

We thank Dr. Pat Card and Dr. Lynn Enquist for the viral strains and Dr. Card and Dr. Gary Pickard for their helpful consultation throughout these studies. We also thank Leslie Gillum, Wendy Irelan, Cristel Merrouche, and Greg Tennant for technical assistance, Ian Morris for photographic help, and Elizabeth Downes for editorial comments.

### LITERATURE CITED

- Argamaso, S.M., M.K. Knowlton, and R.G. Foster (1993) Photoreception and circadian behavior in *rd* and *rd/s* mice. *Invest. Ophthalmol. Visual Sci. Suppl.* 34:1077.
- Balkema, G.W. and U.C. Drager (1990) Origins of uncrossed retinofugal projections in normal and hypopigmented mice. *Vis. Neurosci.* 4:595–604.
- Bowes, C. and D.B. Farber (1987) mRNAs coding for proteins of the cGMP cascade in the degenerative retina of the *rd* mouse. *Exp. Eye Res.* 45:467–480.
- Bowes, C., T. van Veen, and D.B. Farber (1988) Opsin, G-protein and 48-kDa protein in normal and *rd* mouse retinas: Developmental expression of mRNAs and protein and light/dark cycling of mRNAs. *Exp. Eye Res.* 47:369–390.
- Bowes, C., M. Danciger, C.A. Kozak, and D.B. Farber (1989) Isolation of a candidate cDNA for the gene causing retinal degeneration in the *rd* mouse. *Proc. Natl. Acad. Sci. U.S.A.* 86:9722–9726.
- Bowes, C., T. Li, M. Danciger, L.C. Baxter, M.L. Applebury, and D.B. Farber (1990) Retinal degeneration in the *rd* mouse is caused by a defect in the beta subunit of rod cGMP-phosphodiesterase. *Nature* 347:677–680.
- Card, J.P. and L.W. Enquist (1995) The neurovirulence of pseudorabies virus. *Crit. Rev. Neurobiol.* 9:137–162.
- Card, J.P., L. Rinaman, J.S. Schwaber, R.R. Miselis, M.E. Whealy, A.K. Robbins, and L.W. Enquist (1990) Neurotropic properties of pseudorabies virus: Uptake and transneuronal passage in the rat central nervous system. *J. Neurosci.* 10:1974–1994.
- Card, J.P., M.E. Whealy, A.K. Robbins, R.Y. Moore, and L.W. Enquist (1991) Two alpha-herpesvirus strains are transported differentially in the rodent visual system. *Neuron* 6:957–969.
- Card, J.P., M.E. Whealy, A.K. Robbins, and L.W. Enquist (1992) Pseudorabies virus envelope glycoprotein gI influences both neurotropism and virulence during infection of the rat visual system. *J. Virol.* 66:3032–3041.
- Card, J.P., J.R. Dubin, M.E. Whealy, and L.W. Enquist (1995) Influence of infectious dose upon productive replication and transsynaptic passage of pseudorabies virus in rat central nervous system. *J. Neurovirol.* 1:349–358.
- Carter-Dawson, L., M.M. LaVail, and R.L. Sidman (1978) Differential effects of the *rd* mutation on rods and cones in the mouse retina. *Invest. Ophthalmol. Vis. Sci.* 17:489–498.

- Cassone, V.M., J.C. Speh, J.P. Card, and R.Y. Moore (1988) Comparative anatomy of the mammalian hypothalamic suprachiasmatic nucleus. *J. Biol. Rhythms* 3:71-91.
- Chang, G.Q., Y. Hao, and F. Wong (1993) Apoptosis: Final common pathway of photoreceptor death in *rd*, *rd<sub>s</sub>*, and rhodopsin mutant mice. *Neuron* 11:595-605.
- Clarke, R.J. and H. Ikeda (1985) Luminance and darkness detectors in the olivary and posterior pretectal nuclei and their relationship to the pupillary light reflex in the rat. I. Studies with steady luminance levels. *Exp. Brain Res.* 57:224-232.
- Colwell, C.S. and R.G. Foster (1992) Photic regulation of Fos-like immunoreactivity in the suprachiasmatic nucleus of the mouse. *J. Comp. Neurol.* 324:135-142.
- Cooper, H.M., M. Herbin, and E. Nevo (1993a) Ocular regression conceals adaptive progression of the visual system in a blind subterranean mammal. *Nature* 361:156-159.
- Cooper, H.M., M. Herbin, and E. Nevo (1993b) Visual system of a naturally microphthalmic mammal: The blind mole rat, *Spalax ehrenbergi*. *J. Comp. Neurol.* 328:313-350.
- Cooper, H.M., A. Tessonneaud, A. Caldani, A. Locatelli, S. Richard, and M.C. Viguier-Martinez (1993c) Morphology and distribution of retinal ganglion cells (RGC) projecting to the suprachiasmatic nucleus in the sheep. *Soc. Neurosci. Abstr.* 19:701.11.
- Dolivo, M., E. Beretta, V. Bonifas, and C. Foroglou (1978) Ultrastructure and function in sympathetic ganglia isolated from rats infected with pseudorabies virus. *Brain Res.* 140:111-123.
- Dräger, U.C. and J.F. Olsen (1980) Origins of crossed and uncrossed retinal projections in pigmented and albino mice. *J. Comp. Neurol.* 191:383-412.
- Dreher, B., A.J. Sefton, S.Y. Ni, and G. Nisbett (1985) The morphology, number, distribution and central projections of class I retinal ganglion cells in albino and hooded rats. *Brain Behav. Evol.* 26:10-48.
- Ebihara, S. and K. Tsuji (1980) Entrainment of the circadian activity rhythm to the light cycle: Effective light intensity for a zeitgeber in the retinal degenerate C3H mouse and normal C57BL mouse. *Physiol. Behav.* 24:523-527.
- Enquist, L.W., J. Dubin, M.E. Whealy, and J.P. Card (1994) Complementation analysis of pseudorabies virus gE and gI mutants in retinal ganglion cell neurotropism. *J. Virol.* 68:5275-5279.
- Farber, D.B. and R.N. Lolley (1974) Cyclic guanosine monophosphate: Elevation in degenerating photoreceptor cells of the C3H mouse retina. *Science* 186:449-451.
- Farber, D.B. and R.N. Lolley (1977) Light-induced reduction in cyclic GMP of retinal photoreceptor cells *in vivo*: Abnormalities in the degenerative diseases of RCS rats and *rd* mice. *J. Neurochem.* 28:1089-1095.
- Farber, D.B., S. Park, and C. Yamashita (1988) Cyclic GMP-phosphodiesterase of *rd* retina: Biosynthesis and content. *Exp. Eye Res.* 46:363-374.
- Farber, D.B., C. Bowes, and M. Danciger (1991) Studies leading to the isolation of a cDNA for the gene causing retinal degeneration in the *rd* mouse. *Prog. Clin. Biol. Res.* 362:67-86.
- Farber, D.B., J.S. Danciger, and G. Aguirre (1992) The beta subunit of cyclic GMP phosphodiesterase mRNA is deficient in canine rod-cone dysplasia 1. *Neuron* 9:349-356.
- Follenius, E. and M.P. Dubois (1979) Differentiation immunocytologique de l'innervation hypophysaire de la Carpe à l'aide de serums anti met-enkephaline et anti-alpha-endorphine. *C. R. Seances Acad. Sci. D* 288:639-642.
- Foster, R.G. (1996) The regulation of mammalian circadian rhythms by light. In M.F. Holick and E.G. Jung (ed): *Biologic Effects of Light*. New York: Walter de Gruyter, pp. 372-379.
- Foster, R.G., I. Provencio, D. Hudson, S. Fiske, W. De Grip, and M. Menaker (1991) Circadian photoreception in the retinally degenerate mouse (*rd/rd*). *J. Comp. Physiol. A* 169:39-50.
- Foster, R.G., S. Argamaso, S. Coleman, C.S. Colwell, A. Lederman, and I. Provencio (1993) Photoreceptors regulating circadian behavior: A mouse model. *J. Biol. Rhythms* 8:S17-S23.
- Gibson, A.R., D.I. Hansma, J.C. Houk, and F.R. Robinson (1984) A sensitive low artifact TMB procedure for the demonstration of WGA-HRP in the CNS. *Brain Res.* 298:235-241.
- Goodman, C.S. and C.J. Shatz (1993) Developmental mechanisms that generate precise patterns of neuronal connectivity. *Cell* 72:77-98.
- Gustafson, D.P. (1975) Pseudorabies. In H.W. Dunne and A.D. Leman (ed): *Diseases of Swine*. Ames: Iowa State University Press, pp. 209-223.
- Harrington, M.E. and B. Rusak (1991) Luminance coding properties of intergeniculate leaflet neurons in the golden hamster and the effects of chronic clorgyline. *Brain Res.* 554:95-104.
- Hickey, T.L. and P.D. Spear (1976) Retinogeniculate projections in hooded and albino rats: An autoradiographic study. *Exp. Brain Res.* 24:523-529.
- Kaprielian, Z. and P.H. Patterson (1994) The molecular basis of retinotectal topography. *BioEssays* 16:1-11.
- Lem, J., J.G. Flannery, T. Li, M.L. Applebury, D.B. Farber, and M.I. Simon (1992) Retinal degeneration is rescued in transgenic *rd* mice by expression of the cGMP phosphodiesterase beta subunit. *Proc. Natl. Acad. Sci. U.S.A.* 89:4422-4426.
- Mason, C.A. and D.W. Lincoln (1976) Visualization of the retino-hypothalamic projection in the rat by cobalt precipitation. *Cell Tissue Res.* 168:117-131.
- McLaughlin, M.E., M.A. Sandberg, E.L. Berson, and T.P. Dryja (1993) Recessive mutations in the gene encoding the beta subunit of rod phosphodiesterase in patients with retinitis pigmentosa. *Nature Genet.* 4:130-134.
- McLaughlin, M.E., T.L. Ehrhart, E.L. Berson, and T.P. Dryja (1995) Mutation spectrum of the gene encoding the beta subunit of rod phosphodiesterase among patients with autosomal recessive retinitis pigmentosa. *Proc. Natl. Acad. Sci. U.S.A.* 92:3249-253.
- Meijer, J.H., G.A. Groos, and B. Rusak (1986) Luminance coding in a circadian pacemaker: The suprachiasmatic nucleus of the rat and the hamster. *Brain Res.* 382:109-118.
- Meijer, J.H., B. Rusak, and G. Ganshirt (1992) The relation between light-induced discharge in the suprachiasmatic nucleus and phase shifts of hamster circadian rhythms. *Brain Res.* 598:1-2.
- Mesulam, M.M. (1978) Tetramethyl benzidine for horseradish peroxidase neurohistochemistry: A non-carcinogenic blue reaction product with superior sensitivity for visualizing neural afferents and efferents. *J. Histochem. Cytochem.* 26:106-117.
- Mettenleiter, T.C. (1991) Molecular biology of pseudorabies (Aujeszky's disease) virus. *Comp. Immunol. Microbiol. Infect. Dis.* 14:151-163.
- Millhouse, O.E. (1977) Optic chiasm collaterals afferent to the suprachiasmatic nucleus. *Brain Res.* 137:351-355.
- Mills, S.L. and S.C. Massey (1995) Differential properties of two gap junctional pathways made by AII amacrine cells. *Nature* 377:734-737.
- Moller, M., J.D. Mikkelsen, J. Fahrenkrug, and H.W. Korf (1985) The presence of vasoactive intestinal polypeptide (VIP)-like-immunoreactive nerve fibres and VIP-receptors in the pineal gland of the Mongolian gerbil (*Meriones unguiculatus*). An immunohistochemical and receptor-autoradiographic study. *Cell Tissue Res.* 241:333-340.
- Moore, R.Y. and N.J. Lenn (1972) A retinohypothalamic projection in the rat. *J. Comp. Neurol.* 146:1-14.
- Moore, R.Y., J.C. Speh, and J.P. Card (1995) The retinohypothalamic tract originates from a distinct subset of retinal ganglion cells. *J. Comp. Neurol.* 352:351-366.
- Murakami, D.M., J.D. Miller, and C.A. Fuller (1989) The retinohypothalamic tract in the cat: Retinal ganglion cell morphology and pattern of projection. *Brain Res.* 482:283-296.
- Noell, W.K. (1965) Aspects of experimental and hereditary retinal degeneration. In C.N. Graymore (ed): *Biochemistry of the Retina*. New York: Academic Press, pp. 51-72.
- Parnavelas, J.G., A. Dinopoulos, and S.W. Davies (1989) The central visual pathways. In A. Björklund, T. Hökfelt, and L.W. Swanson (eds): *Integrated Systems of the CNS, part II*. New York: Elsevier Science, pp. 1-129.
- Perry, V.H. (1979) The ganglion cell layer of the retina of the rat: A Golgi study. *Proc. R. Soc. Lond. B* 204:363-375.
- Perry, V.H. and A. Cowey (1979) Changes in the retino-fugal pathways following cortical and tectal lesions in neonatal and adult rats. *Exp. Brain Res.* 35:97-108.
- Pickard, G.E. (1980) Morphological characteristics of retinal ganglion cells projecting to the suprachiasmatic nucleus: A horseradish peroxidase study. *Brain Res.* 183:458-465.
- Pickard, G.E. (1982) The afferent connections of the suprachiasmatic nucleus of the golden hamster with emphasis on the retinohypothalamic projection. *J. Comp. Neurol.* 211:65-83.
- Pickard, G.E. (1985) Bifurcating axons of retinal ganglion cells terminate in the hypothalamic suprachiasmatic nucleus and the intergeniculate leaflet of the thalamus. *Neurosci. Lett.* 55:211-217.

- Pittler, S.J. and W. Baehr (1991a) Identification of a nonsense mutation in the rod photoreceptor cGMP phosphodiesterase beta-subunit gene of the *rd* mouse. *Proc. Natl. Acad. Sci. U.S.A.* *88*:8322–8326.
- Pittler, S.J. and W. Baehr (1991b) The molecular genetics of retinal photoreceptor proteins involved in cGMP metabolism. *Prog. Clin. Biol. Res.* *362*:33–66.
- Portera-Cailliau, C., C.H. Sung, J. Nathans, and R. Adler (1994) Apoptotic photoreceptor cell death in mouse models of retinitis pigmentosa. *Proc. Natl. Acad. Sci. U.S.A.* *91*:974–978.
- Provencio, I. and R.G. Foster (1993) Photoreceptors mediating the regulation of circadian rhythms in *rd/rd* mice. *Invest. Ophthalmol. Vis. Sci. Suppl.* *34*:740.
- Provencio, I. and R.G. Foster (1995) Circadian rhythms in mice can be regulated by photoreceptors with cone-like characteristics. *Brain Res.* *694*:183–190.
- Provencio, I., S. Wong, A.B. Lederman, S.M. Argamaso, and R.G. Foster (1994) Visual and circadian responses to light in aged retinally degenerate mice. *Vis. Res.* *34*:1799–1806.
- Rado, R., H. Gev, and J. Terkel (1988) The role of light in entraining mole rats' circadian rhythms. *Israel J. Zool.* *35*:105–106.
- Rodieck, R.W. and R.K. Brening (1983) Retinal ganglion cells: Properties, types, genera, pathways and trans-species comparisons. *Brain Behav. Evol.* *23*:3–4.
- Rouiller, E.M., M. Capt, M. Dolivo, and F. De Ribaupierre (1986) Tensor tympani reflex pathways studied with retrograde horseradish peroxidase and transneuronal viral tracing techniques. *Neurosci. Lett.* *72*:247–252.
- Rouiller, E.M., M. Capt, M. Dolivo, and F. De Ribaupierre (1989) Neuronal organization of the stapedius reflex pathways in the rat: A retrograde HRP and viral transneuronal tracing study. *Brain Res.* *476*:21–28.
- Scalia, F. (1972) The termination of retinal axons in the pretectal region of mammals. *J. Comp. Neurol.* *145*:223–257.
- Shatz, C.J. (1994) Viktor Hamburger Award review. Role for spontaneous neural activity in the patterning of connections between retina and LGN during visual system development. *Int. J. Dev. Neurosci.* *12*:531–546.
- Standish, A., L.W. Enquist, and J.S. Schwaber (1994) Innervation of the heart and its central medullary origin defined by viral tracing. *Science* *263*:232–234.
- Stone, J. (1978) The number and distribution of ganglion cells in the cat's retina. *J. Comp. Neurol.* *180*:753–771.
- Stone, J. and J.E. Campion (1978) Estimate of the number of myelinated axons in the cat's optic nerve. *J. Comp. Neurol.* *180*:799–806.
- Strack, A.M. and A.D. Loewy (1990) Pseudorabies virus: a highly specific transneuronal cell body marker in the sympathetic nervous system. *J. Neurosci.* *10*:2139–147.
- Strack, A.M., W.B. Sawyer, J.H. Hughes, K.B. Platt, and A.D. Loewy (1989a) A general pattern of CNS innervation of the sympathetic outflow demonstrated by transneuronal pseudorabies viral infections. *Brain Res.* *491*:156–162.
- Strack, A.M., W.B. Sawyer, K.B. Platt, and A.D. Loewy (1989b) CNS cell groups regulating the sympathetic outflow to adrenal gland as revealed by transneuronal cell body labeling with pseudorabies virus. *Brain Res.* *491*:274–296.
- Strick, P.L. and J.P. Card (1992) Transneuronal mapping of neural circuits with alphaherpes virus. In J.P. Bolam (ed): *Experimental Neuroanatomy: A Practical Approach*. Oxford: IRL Press, pp. 81–101.
- Takahashi, J.S., L.H. Pinto, and M.H. Vitaterna (1994) Forward and reverse genetic approaches to behavior in the mouse. *Science* *264*:1724–1733.
- Tiao, Y.C. and C. Blakemore (1976) Regional specialization in the golden hamster's retina. *J. Comp. Neurol.* *168*:439–457.
- Tillet, Y., M. Caldani, and G. Tramu (1989) Immunohistochemical characterization of the sheep suprachiasmatic nucleus. *J. Chem. Neuroanat.* *2*:215–226.
- Trejo, L.J. and C.M. Cicerone (1984) Cells in the pretectal olivary nucleus are in the pathway for the direct light reflex of the pupil in the rat. *Brain Res.* *300*:49–62.
- Vitaterna, M.H., D.P. King, A.M. Chang, J.M. Kornhauser, P.L. Lowrey, J.D. McDonald, W.F. Dove, L.H. Pinto, F.W. Turek, and J.S. Takahashi (1994) Mutagenesis and mapping of a mouse gene, *Clock*, essential for circadian behavior. *Science* *264*:719–725.
- Yamazaki, I. and S. Suga (1969) Studies on retinitis pigmentosa. XXVIII. Rhodopsin contents and ERG findings of experimental retinal degeneration and hereditary retinal dystrophy in mice [Japanese]. *Nippon Ganka Gakkai Zasshi Acta Soc. Ophthalmol. Japon.* *73*:1801–1813.
- Yoshimura, T., M. Nishio, M. Goto, and S. Ebihara (1994) Differences in circadian photosensitivity between retinally degenerate CBA/J mice (*rd/rd*) and normal CBA/N mice (+/+). *J. Biol. Rhythms* *9*:51–60.
- Young, M.J. and R.D. Lund (1994) The anatomical substrates subserving the pupillary light reflex in rats: Origin of the consensual pupillary response. *Neuroscience* *62*:481–496.
- Zamboni, L. and L. de Martino (1967) Buffered picric acid formaldehyde: A new rapid fixative for electron microscopy. *J. Cell Biol.* *35*:148A.